Global dynamics perspective on macro- to nano-mechanics

GLOBAL DYNAMICS PERSPECTIVE ON MACRO- TO NANO-MECHANICS

Giuseppe Rega and Valeria Settimi
Department of Structural and Geotechnical Engineering, Sapienza University of Rome, Rome, Italy
giuseppe.rega@uniroma1.it; valeria.settimi@uniroma1.it

Abstract
In about the last two decades, global nonlinear dynamics has been evolving in a revolutionary way, with the development of sophisticated techniques employing concepts/tools of dynamical systems, bifurcation, and chaos theory, and applications to a wide variety of mechanical/structural systems. The relevant achievements entail a substantial change of perspective in dealing with vibration problems, and are ready to meaningfully affect the analysis, control, and design of systems at different scales, in multiphysics contexts too. After properly framing the subject within some main stages of developments of nonlinear dynamics in solid/structural mechanics, as occurred over the last forty years, the article focuses on highlighting the role played by global analysis in unveiling the nonlinear response and actual safety of engineering systems in different environments. Reduced order models of macro/micro-structures are considered. Global dynamics of a laminated plate with von Kármán nonlinearities, shear deformability, and full thermomechanical coupling allows to highlight the meaningful effects entailed by the slow transient thermal dynamics on the fast steady mechanical responses. An atomic force microcantilever is referred to for highlighting the severe worsening of overall stability associated with the application of an external feedback control, and the importance of global dynamics for conceiving and effectively implementing a control procedure aimed at enhancing engineering safety. The last part of the article dwells on the general role that a global dynamics perspective is expected to play in the safe design of real systems, in the near future, focusing on how properly exploiting concepts and tools of dynamical integrity to evaluate response robustness in presence of unavoidable imperfections, and to improve the system's actual load carrying capacity.

Keywords: Multistability, Global bifurcation, Dynamical integrity, Control, Thermomechanics, Atomic force microscopy, Practical stability, Engineering design

Contents

Abbreviations

AFM	atomic force microscope
BC	boundary crisis
BS	basin stability
DI	dynamical integrity
GIM	global integrity measure
IF	integrity factor
LIM	local integrity measure
MEMS	micro-electro-mechanical-system
nD	n-dimensional
ODE	ordinary differential equation
OGY	Ott-Grebogi-Yorke
PD	period doubling
Pm	m-period solution
ROM	reduced order model
sdof	single-degree-of-freedom
SN	saddle-node

1 Introduction

Global dynamics is a main part of dynamical systems or nonlinear dynamics theory, these being two alternative – but not fully equivalent – terminologies used to identify a wide area of systems' nonlinear science by preferably looking either at its fundamental aspects in rigorous mathematical terms or at a balance between fundamentals and technological outcomes in an applied science and engineering perspective. This article definitely fits into the second framework and focuses on an important part of it, namely the area of solid/structural mechanics into which theoretical accomplishments on the global behaviour of systems, achieved within the physical-mathematical community, have spread out in about the last two decades of the previous century, with a physiological time delay. Thus, dwelling on fundamentals and theoretical developments of global analysis is not in the scope of the present work, and reference to the literature in the background is limited to a small number of textbooks that fueled the knowledge of relevant aspects from a more theoretical [1,2] or application-oriented [3,4] perspective, with also a view to computational issues [5,6].

From the viewpoint of mechanics of solids, machines and structures, and of their engineering applications, interest towards global dynamics grew up since about the beginning of the 90s, when the classical theory of nonlinear oscillations was meaningfully complemented by the use of bifurcation theory for the local and global analysis of complex dynamics. This is illustrated schematically by the chronological chart in Fig. 1, where a summary of nominal stages and time periods of major development of nonlinear dynamics in mechanics over the last forty years is outlined [7]. The figure highlights a progressive transition from the earlier stage of 'nonlinear oscillations' dealt with via analytical (mostly asymptotic) techniques, to the modern stages of 'bifurcation and complex dynamics' addressed via computational and geometrical techniques, on one side, and 'experimental nonlinear dynamics', on the other side. Then ending up to the current 'hybridization' of nonlinear dynamics with a variety of scientific and technological areas where the relevant concepts and phenomena, and the combined and comprehensive use of complementary (analytical, geometrical, computational, and experimental) techniques, allow to interpret and govern a number of technological problems. Figure 1 also outlines the global dynamics context into which the present article is framed, however enriched by the predictive capability of analytical techniques and the validating role of experimental investigations.

Nonlinear dynamic analyses have been conducted in the literature mostly on low-dimensional archetypal models described by very few nonlinear ordinary differential equations (ODEs). Often, minimal (single-degree-of-freedom (sdof) or single-mode) model have been considered to represent the dynamic behaviour of a variety of actually discrete mechanical systems or of non-internally resonant continuous structures discretized via some reduction technique, e.g. the standard Galerkin procedure with assumed shape functions

(commonly linear modes, but also possibly proper orthogonal modes or nonlinear normal modes). In an increasing number of cases, proper reduced order models (ROMs) have been formulated by also exploiting hints provided by experimental investigations on small-scale physical models as to the kind and number of active dof/modes taking meaningful part in the structural response to a possibly resonant external and/or parametric excitation. As a matter of fact, if succeeding in identifying a reliable ROM for the analysis and description of system dynamics in given conditions, low-dimensional models are the sole ones which the quite sophisticated analytical, geometrical, and computational techniques of global analysis can be applied to in an affordable and effective way. Within such a dimension reduction context, local bifurcation analysis is often paralleled by a companion global analysis, generally based on pursuing the construction of basins of attraction that provide a more complete description of bifurcation and response scenarios. This is important mostly due to the multistable nature of nonlinear systems for a given set of parameters, with the knowledge of all possible solutions being crucial for their reliability and safety. The number of coexisting solutions meaningfully depends on the type of nonlinearity, the number of dof, and the type of coupling between subsystems, and strongly varies when parameter values change. The considerable amount of studies on multistability and, more generally, on global dynamics of systems, with a variety of specifically addressed items of either theoretical or numerical nature, prevents us from quoting even a few of them. Yet, in all considered cases, analysis of global features of the response has definitely allowed to enhance the overall understanding of systems' nonlinear dynamics, although often in an essentially incremental way.

However, based on powerful concepts and tools of dynamical systems, bifurcation, and chaos theory, in about the last three decades global nonlinear dynamics has been evolving in such a revolutionary way to entail a wider perspective, and a possible change of paradigm, for the analysis, control and design of mechanical and structural systems. Accordingly, it is now deemed ready to significantly influence also the reliable assessment of systems' actual load carrying capacity. The present feature article builds on this renewed ground, and aims at making a step forward along the global dynamics perspective by presenting and discussing cases in which the local bifurcation analysis of systems has to be properly complemented with a companion global analysis in order not to miss fundamental aspects of the overall response. The focus is thus on the role played by global dynamics in unveiling a variety of issues in the analysis, control and overall safety of engineering systems from macro- to micro/nano-mechanics, even in a possibly multiphysics context.

Nonlinear dynamics of a structure in a multifield macro-mechanics environment is indeed the first case study addressed in the paper (Sect. 2), in the response analysis perspective. A minimal model of composite plate with von Kármán nonlinearities, shear deformability, and two-way thermomechanical coupling, subjected to thermal boundary excitations that induce buckling, in addition to a harmonic, transverse, mechanical excitation, is investigated via local and global analysis. The latter proves to be essential for unveiling the meaningful effects steadily entailed on the fast mechanical response by the slow transient thermal dynamics.

Then, a few basic items of global analysis of systems are summarized, including invariant manifolds of Hamiltonian saddles, their perturbation in damped and forced conditions, and the ensuing homo/heteroclinic bifurcations. The topological role played by the latter in the onset of complex dynamics attained through the erosion of basins of attraction of regular solutions is discussed, along with its ending up with the escape of system dynamics from a safe potential well (Sect. 3.1). Of course, all addressed issues are well known, and

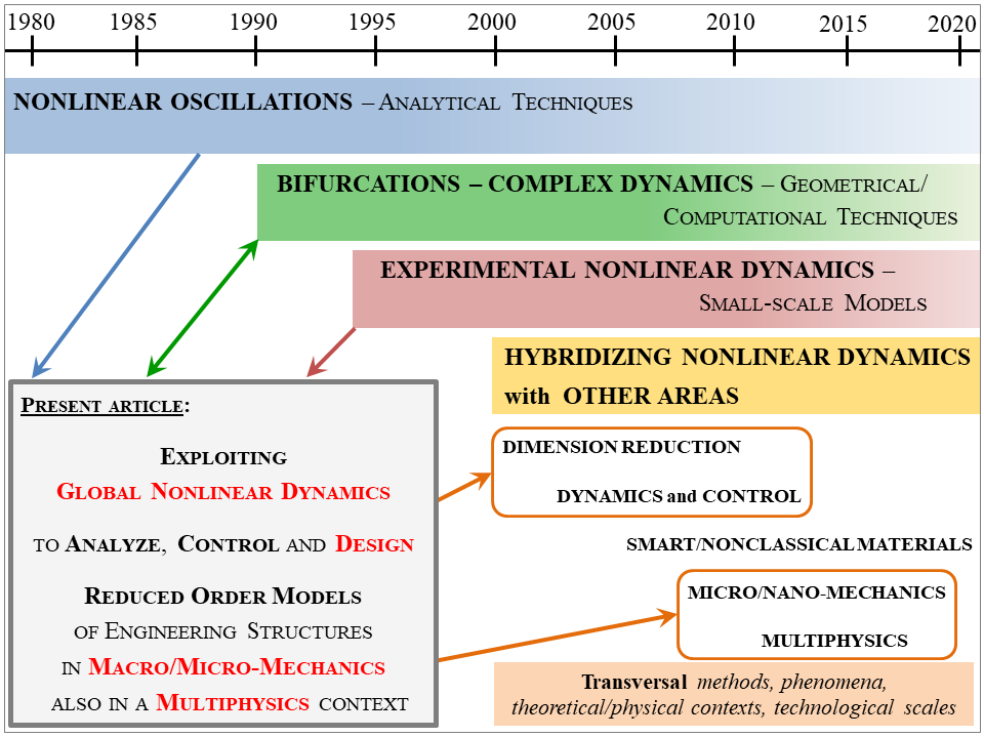

Fig. 1 Framing the present feature article within historical stages of development of nonlinear dynamics in mechanics. (Colour figure online)

their illustration has to be intended just as a remind of the context into which successive analyses, discussions and outcomes are to be framed. Section 3.2 summarizes the conceptual and operational steps of dynamical integrity as a geometrical-computational approach to the global analysis of systems, aimed at their safety evaluation, with reference to a variety of mechanical, dynamical and bifurcation aspects. The possibility to control the underlying global events by exploiting concepts and analytical techniques of nonlinear dynamics, and its effects on the dynamical integrity, are dealt with in Sect. 3.3, while Section 3.4 summarizes the features of the basin stability method as a purely computational approach to global analysis.

Issues of analysis, control and safety evaluation are presented in more detail for a single-mode model of noncontact Atomic Force Microscope (AFM) cantilever, to be considered as a suitable illustrative system susceptible to undergo dynamical escape in micro/nano-mechanics. Moving from the local and global analysis of the reference system response, global effects of two different control techniques are summarized. First, the unsafe overall dynamics ensuing from an external feedback control even properly tailored for response stabilization purposes is highlighted (Sect. 4.1). Then, the enhancement of system dynamical robustness against escape, achievable via careful numerical identification of the governing bifurcational event and proper implementation of the control technique based on global dynamics, is dealt with (Sect. 4.2).

The last part of the paper dwells with the general role played by global analysis for a reliable stability evaluation and safe engineering design. First, the practical stability of systems – as ensuing from imperfections, small but finite dynamical perturbations, variations of control parameters, or even possible uncertainties in the system and excitation features – is contrasted with the higher theoretical (Lyapunov) stability, solely accounting for the system's local dynamics, which is generally assumed to govern its load carrying capacity (Sect. 5.1). Then, the capability of two different (basin stability and dynamical integrity) approaches for the evaluation of systems' robustness and safety is addressed, looking both at the effects of the relevant, always underlying, stochasticity and at the conceptual and operational difficulties encountered when moving to the higher-dimensional models needed to describe the nonlinear dynamics of real structures (Sect. 5.2). Last, it is discussed how dynamical integrity may pave the way towards a (definitely lengthy, yet

fundamental) process of revision of current design criteria generally overlooking nonlinear and, mostly, global dynamical effects. This may lead to a novel paradigm for safe and aware engineering design in which the performance and effectiveness of mechanical systems and structures can be meaningfully, yet consciously, enhanced, with expectable overall advancements in structural conception, technological development, and cost reduction (Sect. 5.3).

2 Exploiting global dynamics for analysis: a thermomechanically coupled plate

Among the variety of multiphysics phenomena which are becoming increasingly important in a wide class of technological applications, thermomechanical coupling of materials and structures in a nonlinear dynamics environment represents a topic of great interest in fields like aerospace engineering, civil and mechanical engineering, and in micro-electro-mechanics. In the context of a global dynamics investigation, low-order models able to preserve the main features of the underlying continuum formulations turn out to be crucial to perform the nonlinear analyses in a reduced state space, still with the possibility to obtain fundamental insight into thermal-structural interactions.

The thermomechanical plate model here used is derived within a unified modeling framework integrating mechanical and thermal aspects which, starting from the three-dimensional physics problem, moves to the two-dimensional and zero-dimensional formulations, as presented in [8], to be referred for all details. Assumptions of third order shear deformability and consistent cubic temperature variation along the thickness are imposed, and, in absence of internal resonance between the plate transverse modes, a single-mode Galerkin approximation is adopted for the transverse displacement and the two independent bending and membrane temperatures. Statical condensation of the in-plane displacements components, nondimensionalization with respect to time, plate thickness, and external frequency, set at primary resonance, and the choice of a dome-shaped prescribed temperature on the upper and lower surfaces, allow to obtain the following three coupled nonlinear ODEs for an orthotropic single-layer simply supported plate (Fig. 2) with movable and isothermal edges

$$\ddot{W}(t) + a_{12}\dot{W}(t) + a_{13}W(t) + a_{14}W(t)^3 + a_{15}T_{R1}(t) + a_{16}T_{R0}(t)W(t) + a_{17}Cos(t) + a_{18}(T_{up} + T_{down})W + a_{19}(T_{up} - T_{down}) = 0 \tag{1a}$$

$$\dot{T_{R0}}(t) + a_{22}T_{R0}(t) + a_{23}\alpha_1(T_{up} + T_{down}) + a_{24}W(t)\dot{W}(t) + a_{25}e_0(t) = 0 \tag{1b}$$

$$\dot{T_{R1}}(t) + a_{32}T_{R1}(t) + a_{33}\dot{W}(t) + a_{34}e_1(t) + a_{35}\alpha_1(T_{up} - T_{down}) = 0\,, \tag{1c}$$

in terms of the 0D configuration nondimensional reduced variables W (deflection of the plate center), T_{R0} (membrane temperature), T_{R1} (bending temperature) [9]. T_{up} and T_{down} are the central values of the dome-shape temperature prescribed on the upper and lower external surfaces, respectively, e_0 and e_1 are the membrane and

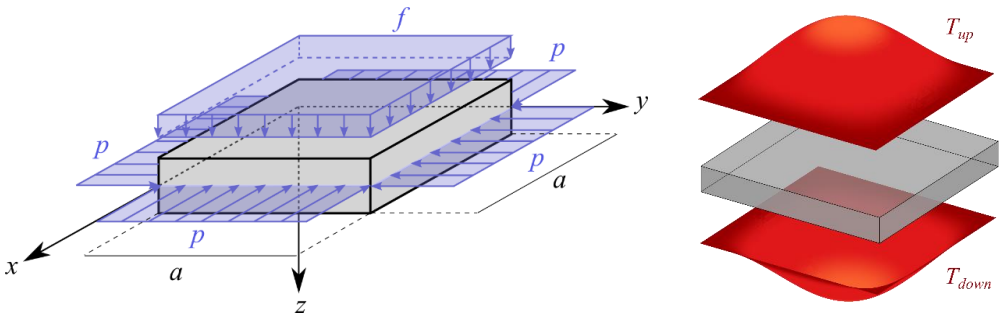

Fig. 2 Square single-layer plate subjected to mechanical (blue) and thermal (red) loads. (Colour figure online)

bending heat sources inside the plate, and dot denotes the time derivative. The dynamical behaviour of the thermomechanically coupled model is studied by considering an epoxy/carbon fiber square composite plate with aspect ratio h/a =1/100. The subsequent nondimensional numerical coefficients a_{ij} are reported in [9]. The mechanical loads applied to the plate are represented by an in-plane pre-stressing force p = 2.51, corresponding to a condition of incipient buckling, and a low transversal resonant harmonic excitation (f =1), included in the a_{13} = 1-p and a_{17} = -f coefficients, respectively. As concerns the thermal loads, a generic condition of different temperatures prescribed on the external plate surfaces is considered, i.e. T_{up} = 300 K and T_{down} = 100 K, without presence of heat sources inside the plate. It is worth noting that this kind of thermal boundary condition affects all three equations, furnishing an external contribution to the dynamics of membrane and bending temperatures, and acting on the mechanical dynamics through external and parametric terms. In the latter, combination with the coupling terms can crucially modify the mechanical response potentially inducing buckling [9].

2.1 Slow transient thermal effects in the swift steady structural response

Starting from local dynamics analysis, the bifurcation diagram in Fig. 3a shows the evolution of the stationary mechanical response, in terms of minimum and maximum values of the displacement W, for varying

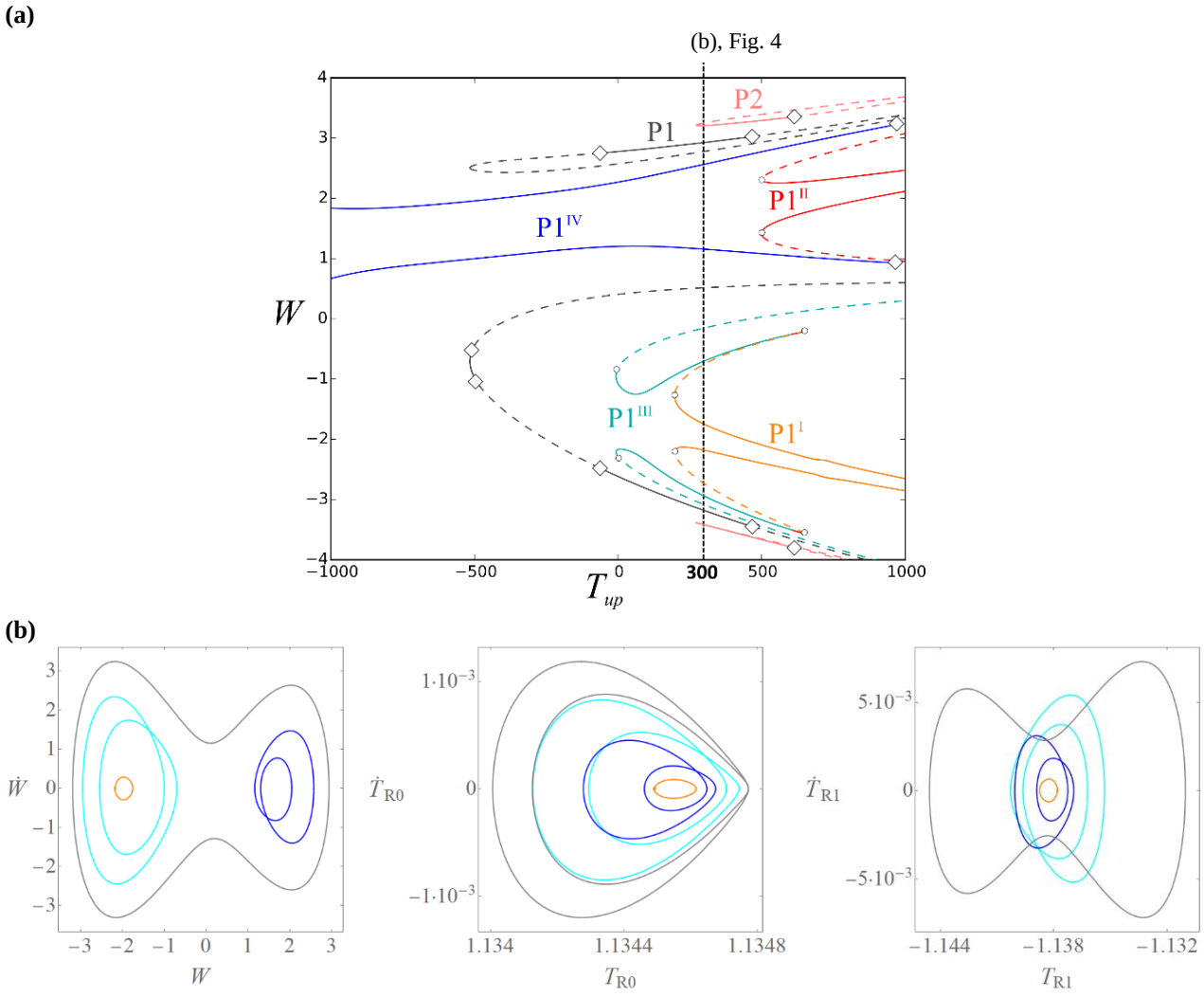

Fig. 3 Bifurcation diagrams of displacement as a function of the temperature on the upper surface T_{up}, for p = 2.51, T_{down} = 100 K **(a)**; phase portraits of the 1-period solutions at T_{up} = 300 **(b)**. Circle: saddle-node bifurcation; Diamond: period-doubling bifurcation. (Colour figure online)

temperature on the upper surface, with fixed T_{down} = 100 K. The outcomes, obtained via continuation technique with software AUTO [10], show a variety of 1-period motions around the varied positive and negative buckled configurations of the plate (i.e., in one of the two potential wells, in global dynamics terms), characterized with phase portraits and Poincaré maps in Fig. 3b, for T_{up} = 300 K. They coexist, in a limited range, with the P1 (gray) solution oscillating around both buckled equilibria, which represents the sole existing solution in the pre-buckling regime [9]. Due to the activation of $a_{15}T_{R1}(t)$ and $a_{19}(T_{up} - T_{down})$ terms in Eq. (1a), the system displays different behaviours around the bucked equilibria, with two couples of low-amplitude ($P1^{I}/P1^{II}$) and high-amplitude ($P1^{III}/P1^{IV}$) solutions existing in different temperature ranges, with also different amplitudes, as shown in left panel of Fig. 3b. Furthermore, a 2-period P2 solution oscillating around both equilibria is detected. Looking at the response of the thermal variables (central and right panels of Fig.3b), their very limited oscillations (induced by the presence of coupling with mechanical displacement in Eqs. (1b,c)) occur around the steady values T_{R0} = 1.13454 and T_{R1} = -1.13818, and the relevant bifurcation diagrams (not reported here for the sake of conciseness) are organized along a straight line, due to the nearly linear nature of the thermal equations.

To obtain a comprehensive description of the response scenario, global dynamics is also accomplished by analyzing the system basins of attraction via an ad hoc routine in C++ language, which works by dividing the state plane in a suitably dense grid and by following trajectories starting from the centers of the grid box via quasi-Newton's method. Since the thermomechanical model (1) is four-dimensional in the state space, evaluation of the relevant basins of attraction, and their representation, constitute a computationally demanding task, which is addressed by realizing cross-sections in the mechanical variables plane ($W, \dot{W}$) by considering naturally vanishing initial conditions of the thermal variables, i.e., $T_{R0}(0) = T_{R1}(0) = 0$. Figure 4a shows the basin organization for T_{up} = 300 K and T_{down} = 100 K, i.e. the same configuration analyzed in Fig. 3b. However, comparing the outcomes from local and global analyses, meaningful differences can be pointed out. In fact, the global scenario appears dominated by the buckled high-amplitude cyan $P1^{III}$ response, with also fractalized presence of the P1 gray cross-well solution, while no evidence of orange and pink basins of the $P1^{I}$ and P2 solutions is observed in the basin cross-section, and the basin of the blue $P1^{IV}$ response is extremely fractalized. To understand the reason behind this discrepancy, it is useful to investigate also the global dynamics of the uncoupled 2D model represented by the sole mechanical equation (1a), in which the thermal contributions are introduced in terms of mean steady state values of the relevant variables, T_{R0} = 1.13454 and T_{R1} = -1.13818, derived from the solution of the (uncoupled) thermal equations (1b) and (1c). The cross-section of the relevant basins of attraction is shown in Fig. 4b, and displays a strongly different behaviour, with dominance of the buckled orange $P1^{I}$ and blue $P1^{IV}$ solutions inside the two wells, presence of the 2-period P2 basin, coherently with the outcomes furnished by the local analysis, and a surrounding fractal organization. Comparison of

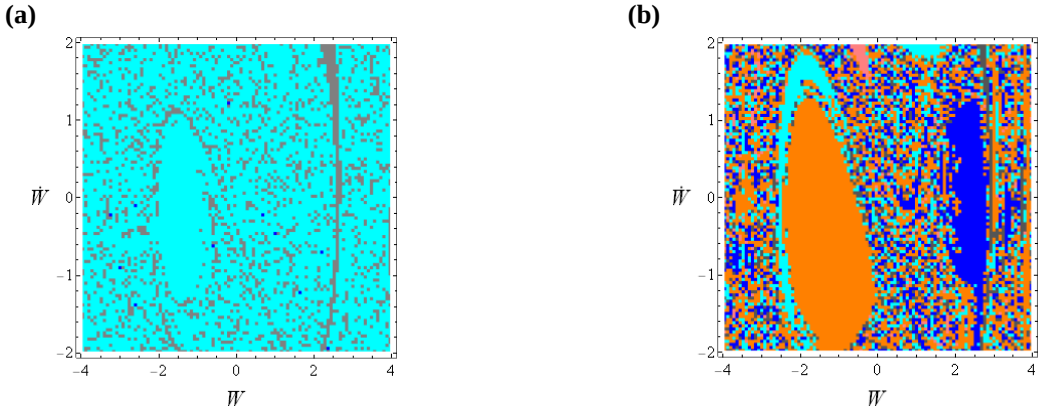

Fig. 4 2D cross-section in the mechanical plane of the basins of attraction for the thermomechanical model with T_{up} = 300 K, T_{down} = 100 K and $T_{R0}(0) = T_{R1}(0) = 0$ **(a)**, basins of attraction of the relevant uncoupled model **(b)**. Gray basin, P1 solution; Orange basin, $P1^{I}$ solution; Cyan basin, $P1^{III}$ solution; Blue basin, $P1^{IV}$ solution; Pink basin, P2 solutions. (Colour figure online)

results of coupled and uncoupled models highlights the crucial role played by the thermal transient in modifying the plate mechanical response. Indeed, both local dynamics and uncoupled model intrinsically neglect it, as continuation analyses are focused on the evolution of stationary responses, thus ignoring mechanical as well as thermal transients, and in the uncoupled model, although accounting for the mechanical transient, the thermal contribution is included into the mechanical evolution just as steady value. Conversely, global dynamics of the fully coupled system naturally considers both mechanical and thermal transient dynamics, thus representing the most suitable tool to comprehensively describe the response of the thermomechanical plate. Time histories of trajectories evolving in the negative well (i.e., with negative mechanical initial conditions $(W, \dot{W}) = (-1.5, -2)$) of Fig. 5 help to clarify the issue. In fact, comparing the evolution of mechanical and thermal variables of the coupled system (cyan line), it is evident that the mechanical dynamics is much faster than the thermal ones, which in turn settle to steady values at different times due to the different order of magnitude of the linear stiffness coefficients $a_{22} = 5.18 \times 10^{-4}$, $a_{32} = 2.59 \times 10^{-3}$ in Eqs. (1b,c). As a consequence, the long transient needed by thermal variables to reach their steady values furnishes a slow contribution to the mechanical dynamics, which firstly oscillates as the pre-buckling P1 gray solution and then reaches the cyan $P1^{III}$ response, that is the first buckled solution born inside the negative well, as highlighted also by the bifurcation diagram in Fig. 3a. Since this solution still exists at steady regime, the trajectories settled on it do persist also after the conclusion of the thermal evolution, when the whole contribution has been provided to the mechanical equation. Differently, when dealing with the uncoupled model (orange line), the solely existing mechanical dynamics receives the full thermal contribution at the beginning of its evolution, and rapidly converges to the orange $P1^{I}$ solution which dominates the negative well in steady regime.

A more exhaustive description of the basins organization in the state space can be achieved by realizing planar cross-sections for also nontrivial values of the thermal variables. In particular, attention is focused on the membrane temperature T_{R0}, which exhibits the slowest evolution, thus producing a major effect on the mechanical response. Figures 6(a)-(c) display three sections in the mechanical plane for different membrane temperature initial conditions, $T_{R0}(0) = 0.4$ (a), $T_{R0}(0) = 0.8$ (b) and $T_{R0}(0) = 1.13454$ (c). Increasing values of T_{R0} initial conditions succeed in revealing the presence of also other basins of attraction, up to replicating the response of the uncoupled model when the initial condition is set to the relevant regime value, as emphasized by the coincidence of results shown in Fig. 6c and Fig. 4b. The reason lies in the progressive shortening of the still lasting transient dynamics as the T_{R0} initial condition becomes closer to the steady value to be reached, which is reflected in a reduced gap to be covered by the membrane thermal variable.

To summarize this behaviour, it is worth analyzing the 4D basins of attraction via a mixed thermal-mechanical planar section, as in Figs. 6d,e, where the basin cross-section in the $(T_{R0}, \dot{W})$ plane is reported at $T_{R1} = -1.13818$, for $W = -1.5$ and $W = 2.5$, within the buckled negative and positive wells, respectively.

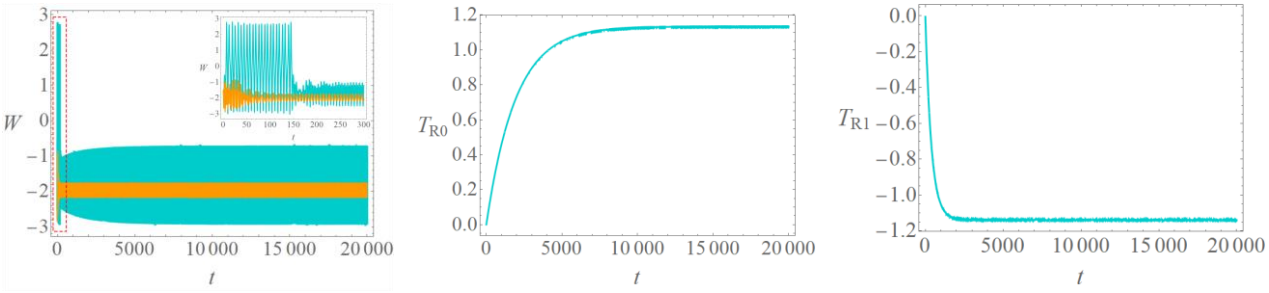

Fig. 5 Time histories of the coupled (cyan) and uncoupled (orange) models, with T_{up} = 300 K, T_{down} = 100 K and i.c. $(W, \dot{W})$ = (-1.5,-2). For the coupled model the thermal i.c. are $T_{R0}(0) = T_{R1}(0) = 0$. (Colour figure online)

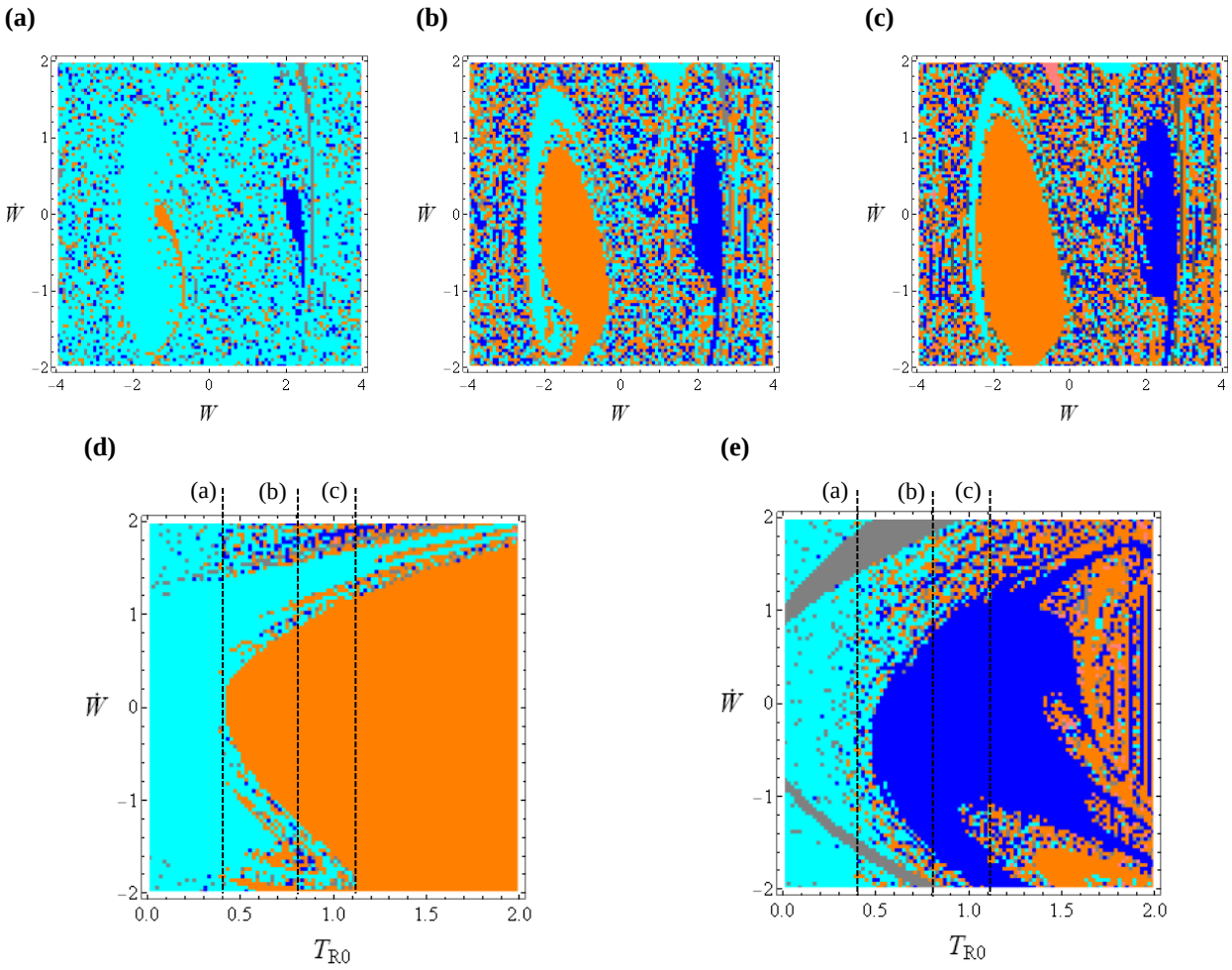

Fig. 6 Coupled model with T_{up} = 300 K, T_{down} = 100 K. Cross-sections of basins of attraction: in the mechanical plane at $T_{R1} = -1.13818$, and $T_{R0} = 0.4$ **(a)**, $T_{R0} = 0.8$ **(b)**, $T_{R0} = 1.13454$ **(c)**; in the $(T_{R0}, \dot{W})$ plane, with $T_{R1} = -1.13818$, at $W = -1.5$ **(d)** and $W = 2.5$ **(e)**. Gray basin, P1 solution; Orange basin, $P1^{I}$ solution; Cyan basin, $P1^{III}$ solution; Blue basin, $P1^{IV}$ solution; Pink basin, P2 solution. (Colour figure online)

For T_{R0} lower than 0.4, the mechanical phase plane of the coupled system is dominated by the negative high-amplitude buckled $P1^{III}$ (cyan) response, with minor fractalized presence of gray P1 and blue $P1^{IV}$ basins, due to the slow thermal contribution in the mechanical equation which is unable to move the response towards the other, also existing, P2 and $P1^{I}$ attractors. The low-amplitude buckled orange $P1^{I}$ basin appears in the negative well and enlarges its compact part for $T_{R0} > 0.4$, while the high-amplitude blue $P1^{IV}$ basin grows up inside the positive well. In terms of steady mechanical outcome of the dynamics this means that, if considering a vanishing initial condition for T_{R0} — as it seems natural from the practical viewpoint — or even a nearly vanishing one within the cyan stripe ($T_{R0} < 0.4$) in the cross-sections of Figs. 6d,e, the coupled system ends up to the high-amplitude negative buckled solution in both wells; instead, assuming $0.4 < T_{R0} < 1.1$, the mechanical response diversifies around the buckled equilibria. For even higher i.c. of T_{R0}, the orange basin becomes dominant inside the negative well, while in the positive one the progression of a strong fractalization meaningfully reduces the magnitude and compactness of the buckled $P1^{IV}$ basin, with undetermined final outcomes.

The results highlight the ability of the coupled model to capture the actual behaviour of the physical system, by taking into account the effects of the thermal slow time evolution on the steady mechanical response, this being a general outcome also occurring if considering different thermal boundary conditions and/or internal heat sources [9]. Indeed, correctly catching coupling effects turns out to be crucially important for all

multiphysics systems, characterized by field variables evolving on different time scales. In contrast, the response of the two-dimensional uncoupled model represents only a partial scenario (i.e., a particular section) of the overall four-dimensional plate behaviour, obtainable with also the coupled model by properly setting the thermal initial conditions to the relevant steady values (thus nullifying the thermal transient). Within the present article's context, it is important to underline that such an involved response scenario, much richer than the peculiar steady one furnished by the local dynamic analysis, can be solely unveiled via a refined global analysis accomplished in the system actual multidimensional phase space.

3 Global analysis: basic phenomenology, dynamical integrity, control, basin stability

3.1 Invariant manifolds, global bifurcations, basins erosion, escape from potential well

To illustrate some key features of global dynamics, reference is made to the classical Helmholtz oscillator, which is the archetypal sdof model describing the dynamics of simple mechanical systems or of ROMs of structures liable to escape. Figure 7 shows (a) a reference mechanical model (the capsizing asymmetric ship) with its motion variable (x), (b) the relevant dimensionless equation of motion with inertia, damping (δ), linear and quadratic elastic restoring forces, and external excitation (γ) terms, (c) the phase portrait of the corresponding Hamiltonian (i.e., unperturbed) system, and (d) the associated potential. Existence of a stable equilibrium position surrounded by bounded oscillation trajectories developing within the potential well is highlighted, along with the invariant manifold of the hilltop saddle beyond which unbounded motions (corresponding to capsizing of the reference mechanical system) occur. The coinciding stable and unstable manifolds of the saddle point are the set of initial conditions that approach the saddle forward and backward in time (t) along its stable and unstable eigenvector, respectively, and represent the system homoclinic orbit. If the stable and unstable manifolds intersect in one point, they intersect in infinitely many points (forward and backward in time). While being structurally unstable sets that cannot be 'observed' directly, invariant manifolds are fundamental stepping stones for the understanding of system dynamics [11]. Indeed, since stable manifolds are boundaries of basins of attractions (which govern the system dynamical integrity), perturbed

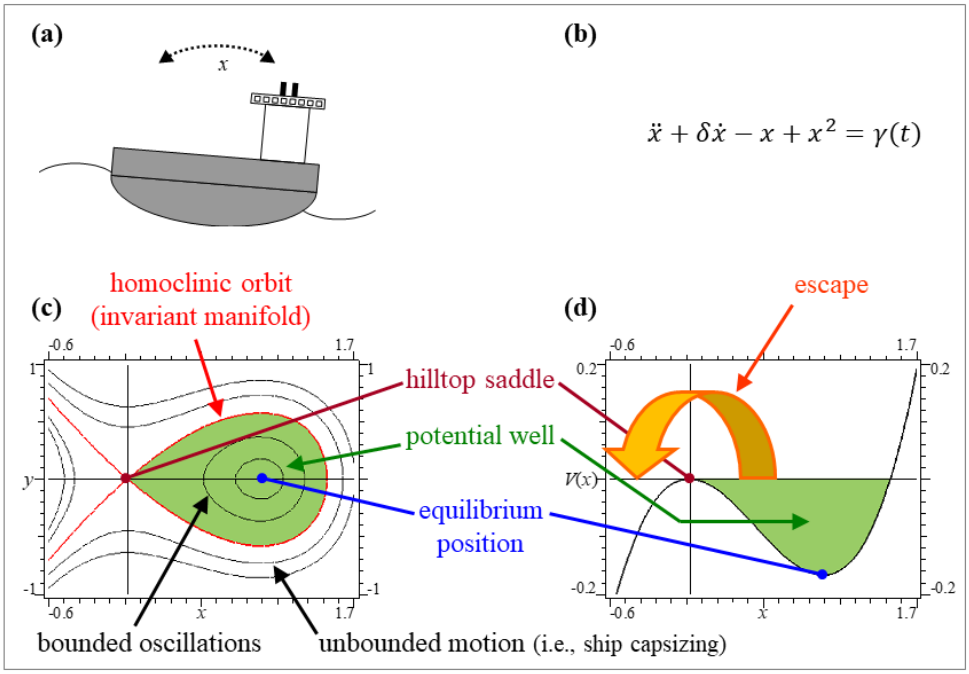

Fig. 7 Helmholtz oscillator: (**a**) reference mechanical model, (**b**) equation of motion, (**c**) phase portrait of the Hamiltonian system, (**d**) the associated potential. (Colour figure online)

invariant manifolds are responsible for fractal basin boundaries when stable and unstable manifolds intersect, and are involved in many topological phenomena.

Following the phenomenological analysis in [12], which is referred to for all details, it is worth shortly dwelling with the effects of damping and excitation, considered as perturbations of the Hamiltonian system governed by the small parameter ε, on the homoclinic orbit. Damping entails separation of the formerly coinciding stable and unstable manifolds (Fig. 8b), with the unstable manifold losing energy in forward time and asymptotically approaching an attractor, and the stable manifold increasing its energy in backward time when approaching the saddle as $t \to +\infty$. There is no more homoclinic loop and a non zero distance between stable and unstable manifolds. This distance is proportional to the small damping amplitude $\varepsilon\delta$ and is approximately constant along a sufficiently short interval. In turn, adding a small but finite harmonic excitation $\gamma(t) = \varepsilon\gamma_1 sin\,(\omega t)$ produces an oscillating distance between the invariant manifolds in the Poincaré map, which in the case of homoclinic bifurcation intersect with each other, as shown in Fig. 8c, where a few primary intersection points (A-D) [2] are marked. The magnitude of the distance is proportional to the excitation amplitude γ_1, and strongly depends on the excitation frequency ω. Overall, the distance between stable and unstable manifolds results from the approximate, additive expression

$$d(m) = \varepsilon\delta a_0 + \varepsilon\gamma_1 a_1(\omega)\cos(m) \tag{2}$$

where, according to physical intuition, damping entails a positive distance between detached manifolds, while

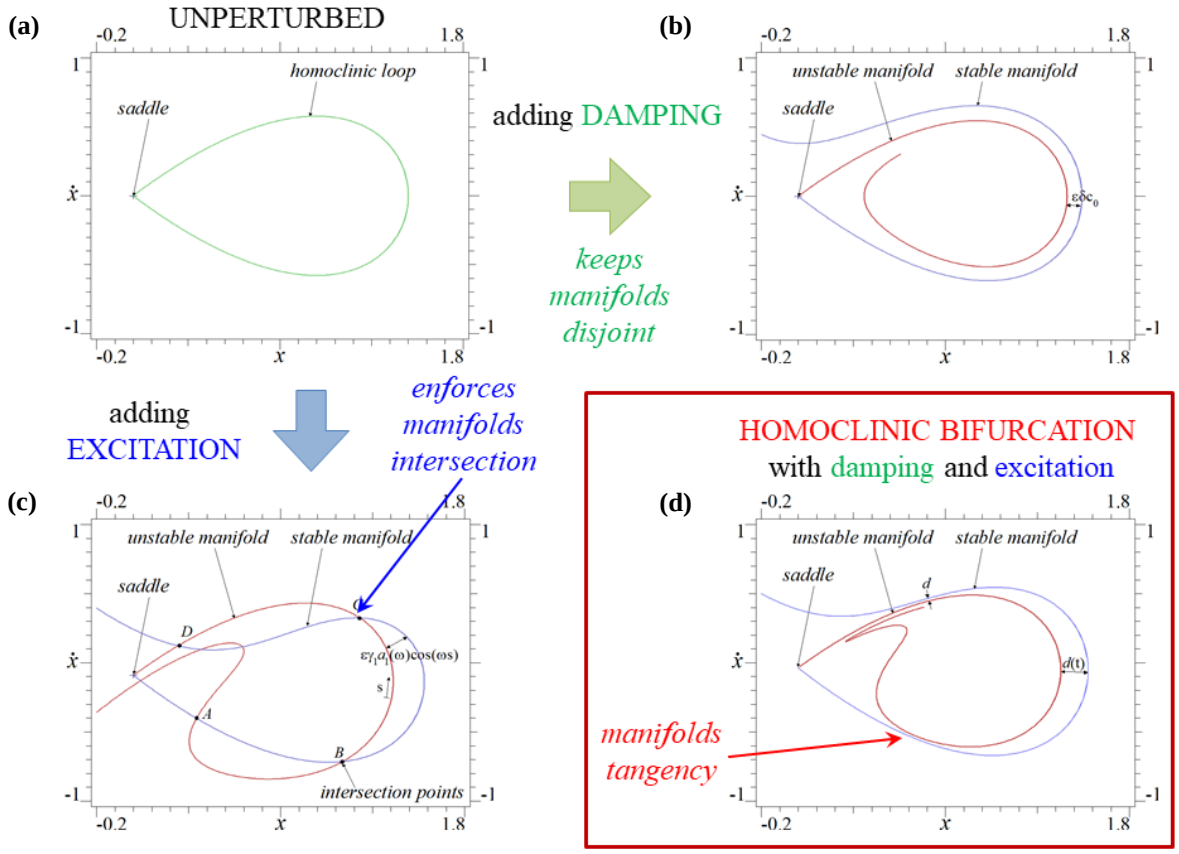

Fig. 8 Schematic illustration of the distances between stable and unstable manifolds. (**a)** Hamiltonian system, (**b)** solely damped system, (**c)** solely harmonically excited system. (**d)** Homoclinic bifurcation with damping and excitation. (Colour figure online)

harmonic excitation entails an oscillating distance which contributes to manifolds intersection. In Eq. (2), the assumed linear dependence of the distance on δ and γ_1 holds only for small damping and excitation amplitude, a_0 and $a_1(\omega)$ are a constant and a function depending on the considered dynamical system, $m=\omega s$, and the cosine is due to the chosen point in Fig. 8c where the arc length parameter s vanishes. Equation (2) is provided by qualitative considerations, but furnishes exact information and the same manifolds distance as obtainable through the Melnikov method [2].

Assuming $a_0 > 0$, if the overall oscillating distance is always positive no manifolds intersection occurs, whereas if it changes sign, i.e. if the minimum distance d between stable and unstable manifolds is negative, intersection occurs. Varying a governing parameter, e.g. the excitation amplitude γ_1, with given excitation frequency, first time vanishing ($d = 0$) of the minimum value of the distance

$$d = \min_{m\in[0,2\pi]}\{d(m)\} = \epsilon\delta a_0 + \varepsilon\gamma_1 a_1(\omega) \min_{m\in[0,2\pi]}\{\cos(m)\} = \epsilon\delta a_0 - \varepsilon\gamma_1 a_1(\omega), \tag{3}$$

corresponds to a tangency between stable and unstable manifolds (Fig. 8d), and marks the occurrence of a homoclinic bifurcation for the critical excitation amplitude $\gamma_{1,cr}^{h}(\omega) = \frac{\delta a_0}{a_1(\omega)}$, with the h upper suffix referring to the considered harmonic excitation. For the reference Helmholtz oscillator, it is $\gamma_{1,cr}^{h}(\omega) = \delta\frac{\sinh(\omega\pi)}{5\pi\omega^2}$ [13].

Homoclinic bifurcation is the global mechanism responsible for (i) starting of fractalization of basin boundaries and sensitivity to initial conditions, (ii) appearance/disappearance of (transient) chaotic attractors or their sudden enlargement/reduction, (iii) triggering phenomena of basins erosion leading more or less suddenly to possibly undesired dynamics. In the case of softening single-well systems (as the Helmholtz oscillator), unwanted dynamics corresponds to unbounded motions occurring after the escape of trajectories from the potential well; in the case of multi-well hardening systems, like the locally softening two-well Duffing oscillator [14], it corresponds to the transition from single-well to cross-well motions. For the Helmholtz oscillator, evolution of phase portraits and associated basins of attraction with increasing excitation amplitude is exemplarily shown in Fig. 9 [13]. Stable and unstable manifolds of the hilltop saddle move from a detached to a tangency, up to a trasverse intersection scenario after the occurrence of homoclinic bifurcation (Fig. 9a). In turn, the coexisting in-well basins evolve from an uneroded scenario at about manifolds tangency to a partially eroded scenario where the manifolds intersect transversally, with the incursion of fractal white tongues from the (unbounded) escape basin into the disappearing green basin, up to a decreasing (i.e., residual) orange basin, with the overall final outcome of the formerly bounded dynamics being the inevitable escape (Fig. 9b). Besides ship capsizing, escape following basins erosion is the extreme dynamical event for a number of systems in macro- and micro/nano-mechanics described by Helmholtz-like oscillators. It corresponds to different kinds of physical failure, which include the unstable dynamic buckling of a variety of slender structures, the dynamic pull-in in micro-electro-mechanical-systems (MEMS) to be used as resonator or sensor devices, and the jump-to-contact in non-contacting atomic force microscopes, to name just a few. Similar manifolds/basins evolutions up to the inevitable escape from a potential well with a varying governing parameter also occur for mechanical systems with multiple hilltop saddles, described by different equations of motion and undergoing heteroclinic bifurcations which involve intersections of manifolds of different saddles: this is the case of, e.g., Duffing-type softening oscillators [15], rocking rigid blocks [16], and the Augusti two-dof model [17].

As regards escape, it is worth noting that, besides a large number of earlier studies made on systems in various theoretical and technological contexts, according to diverse viewpoints and using different techniques, a few ones have been recently devoted to further understanding and clarifying the underlying topological mechanisms (e.g., [18-21]). In the present article, the interest is not in dwelling on the escape phenomenon in itself, nor in addressing the possible variety of associated processes, but only in showing how the in-depth understanding and aware exploitation of basins erosion phenomena in the background of escape may help in the analysis, control and also safe design of engineering systems.

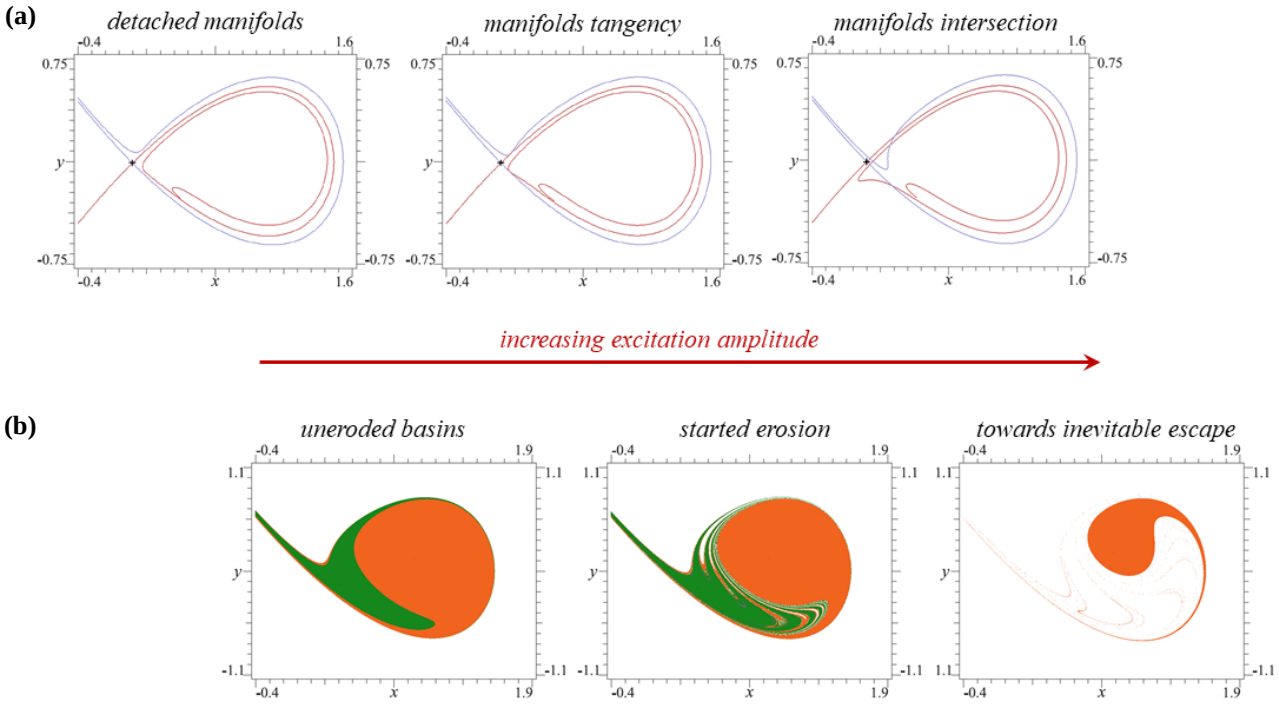

Fig. 9 Helmholtz oscillator. Evolution with increasing excitation amplitude of: **(a)** phase portraits up to homoclinic intersection, **(b)** basins of attraction with erosion (Colour figure online)

3.2 Dynamical integrity: a geometrical-computational approach to global dynamics

Global (homo/heteroclinic) bifurcations entail progressive erosion of basins of attraction, often ending up to final escape of the dynamics. As a matter of fact, the existence of an attractor does not guarantee its practical safety, which strongly depends on the magnitude and the topological features of its basin. In phase space, this must be 'large' and 'compact' (i.e., non-fractal) enough to guarantee robustness of the system dynamical outcome with respect to non-infinitesimal and also infinitesimal variations of the initial conditions, respectively. Moreover, the basin evolution in parameter space must be analyzed in order to ascertain the extent of a possible decrease of response robustness with respect to 'small' variations of system parameters, and its smooth or dangerously sudden features. Indeed, in practice and experiments, variations of both operating initial conditions and parameter values are possible, due to a variety of problem-dependent uncertainties and disturbancies which may entail dynamical outcomes totally different from the theoretically predicted ones.

From a quantitative viewpoint, erosion phenomena and their evolution with a varying control parameter can be analyzed based on the concept of dynamical integrity (DI) and the related operational tools [22]. DI can be considered a *geometrical-computational* criterion to account for the actual shape/structure of basins of attraction and evaluate the stability of the underlying solution, in which calculation is fruitfully paralleled by visualization. With respect to the classical Lyapunov stability, which represents a *local* property of a system attractor, dynamical integrity is a *global* property of the selected dynamical outcome [23,24] representing a substantial widening of perspective which turns out to be essential to safely operate the system with the desired behaviour, depending on expected disturbances. Of course, relying on an in-depth knowledge of system global features, and providing more useful information, it entails specific conceptual difficulties and requires heavy numerical simulations, which for multi-dof systems may become nearly impractical, mostly in connection with the possibility to geometrically represent multidimensional basins of attraction only through specific cross-sections (as made in Sect. 2).

DI analysis is based on the following concepts and related computational tools [24]:

1. Stating accurately the system *safe basin*, i.e. the set of initial conditions in phase space that can be considered safe.
2. Defining *integrity measures* of the safe basin able to quantitatively assess how much the related dynamics is robust with respect to variations of initial conditions.
3. Assessing DI through the construction of *integrity profiles* and *charts* providing all necessary information about how the safe basin evolves due to variations of meaningful system/control parameters.

All three items have been dealt with in a number of papers on DI, with a general overview [25] and the extensive and systematic exposition in [24] being referred to for all details. Here, for each item, just a few aspects are summarized as necessary pre-requisites for an easier understanding of what will be presented and discussed forward.

Overall, the definition of safe basin depends on the 'safe' dynamical condition one wishes to guarantee. Indeed, simply changing the definition of safe basin allows to deal with different features of the system response. Two main distinctions are mentioned. The first depends on being interested in the safety of either (i) the union of the basins of all bounded attractors or (ii) the basin of an individual attractor, belonging to a given potential well, the set of safe initial conditions being those approaching whatever bounded attractor or a specific one inside the well, respectively, as time goes to infinity. The former requirement aims at avoiding out-of-well dynamics, such as escape to infinity (to a neighbouring well) in globally (locally) softening systems like the Helmholtz (two-well Duffing) oscillator [15]. The latter requirement aims at realizing a specifically defined attractor. Cases of both kinds will be dealt with in the sequel. The second distinction is concerned with the interest being in (i) the long-term system behaviour, i.e. in its solely steady dynamics, irrespective of what happens in the transient, or also in (ii) the short-term system behaviour, where its transient response plays a non-trivial role. In the second case, the safe set of initial conditions is clearly a conservative subset of the first one. In the following, steady safe basins will be considered. It is also worth noting that the definitions underlying the above mentioned cases refer to 'nominal' safe basins, which can be non-trivially wider than the 'actual' ones also accounting for (dangerous) basins topology features, as it will be discussed forward.

Several different measures of DI have been proposed in the literature. Indeed, measuring the integrity accurately and properly is a critical point, and a measure may be appropriate in some cases but not in others, strongly depending on the problem to be analyzed, too. Here and in the sequel, three main measures pointing out the transition from a safety conception based on the mere basin width to a perspective of combined width and compactness of the basin, are considered. Indeed, the Global Integrity Measure (GIM), defined as the normalized hypervolume (area in 2D) of the safe basin [26], only accounts for the basin extent, with no care paid to its possible fractality. Thus, while being certainly the most intuitive measure, it may overestimate the actual system DI, being possibly not so reliable. In contrast, both the other two measures eliminate unwanted fractal tongues from the integrity evaluation and only account for the compact part of the safe basin. They are the Local Integrity Measure (LIM) and the Integrity Factor (IF). The former is the normalized radius of the largest hypersphere (circle in 2D) entirely belonging to the safe basin and centered at the attractor [26], the latter is the normalized radius of the largest hypersphere (circle in 2D) entirely belonging to the safe basin [13,27]. While the LIM can be used to evaluate the robustness of long-term individual attractors where the hypersheres are centered, the IF can be used for evaluating the robustness of either a potential well or single competing attractors coexisting within it. A comparative study of IF, GIM, and LIM is reported in [24] where, based on outcomes of a single-mode model of an electrically actuated carbon nanotube [28], they have been shown to work well for evaluating the safety of whatever in-well dynamics against out-of-well phenomena, for estimating the probability of occurrence of a given attractor, and for getting reliable information on its possible practical disappearance in given operational conditions, respectively. Other more general measures also accounting for, e.g., possible inhomogeneous sensitivity of phase space (i.e., displacement and velocity) variables to variations of initial conditions have been used, recently [29].

Of course, a system must be able to sustain changes not only of initial conditions in phase space but also of excitation/system parameters in control space, without changing the desired outcome. An integrity profile

obtained by plotting a DI measure as a function of a driving parameter provides a complete description of the global effects of a single parameter variation in control space [22,30]. Although different profile patterns are possible, in the most common situation of interest from a safety viewpoint the DI typically decreases with increasing excitation amplitude, and the integrity profile plays the role of either the erosion curve of a potential well ending up to final escape of the former in-well dynamics, or the decreasing robustness diagram of a basin of attraction (also possiby keeping its compactness, i.e. undergoing shrinkage but not erosion) ending up to its disappearance and final settling of the dynamics onto a competing attractor. In the following, we focus on the erosion profile of the potential well of a generic (globally or locally) softening system, which is associated with the (variably) sharp reduction of well compactness, due to some global bifurcation event entailing penetration of fractal tongues from a coexisting out-of-well (unconfined or confined) basin, and smooth reductions of its (original or residual) compact extent, overall giving rise to a decrease of robustness of the underlying safe dynamics. Indeed, irrespective of the considered integrity measure (up to a certain extent), three main regions can be identified, in exact or approximate way, in the typical erosion profile of a potential well, as shown by the schematic in Fig. 10: (i) an initial slightly decreasing path, towards the end of which a homoclinic or heteroclinic bifurcation of the manifolds of a hilltop saddle takes place, triggering the safe basin erosion; (ii) a successive fall down occurring for excitation amplitudes variably shifted towards higher values, often in a sharp (i.e., highly dangerous) way; (iii) a second, smoother, further decreasing (and generally short) path, characterized by merely residual and unacceptable values of DI, with the final onset of out-of-well phenomena representing the system physical ‘failure’ in globally softening systems. For parameter values at the onset of the intermediate, sharply decreasing, zone, the erosion may also proceed with quite complex topological mechanisms, possibly involving global bifurcations of the manifolds of some ‘secondary’ saddle.

Following [24], it is worth looking at the three regions in the operational safety perspective. In the left region, the theoretical stability is ensured, i.e. the desired solution exists and is characterized by a very high DI, capable to absorb the effects of the disturbances encountered in real-world applications. The local stability analysis is sufficient to guarantee that the structure safely operates under realistic conditions, and there is no need of a detailed global safety analysis. In the right region, the desired solution no longer exists theoretically and, correspondingly, the DI has vanished. Again, the local stability analysis succeeds in detecting the boundary of its actual disappearance, with no need to resort to the assessment of global safety. The situation is completely different in the intermediate region, where the practical stability is not guaranteed due to the integrity possibly decreasing in a sharp and very dangerous way, although the theoretical stability is ensured. Thus, the desired solution may practically exist only in a left sub-region, also possibly quite smaller than the

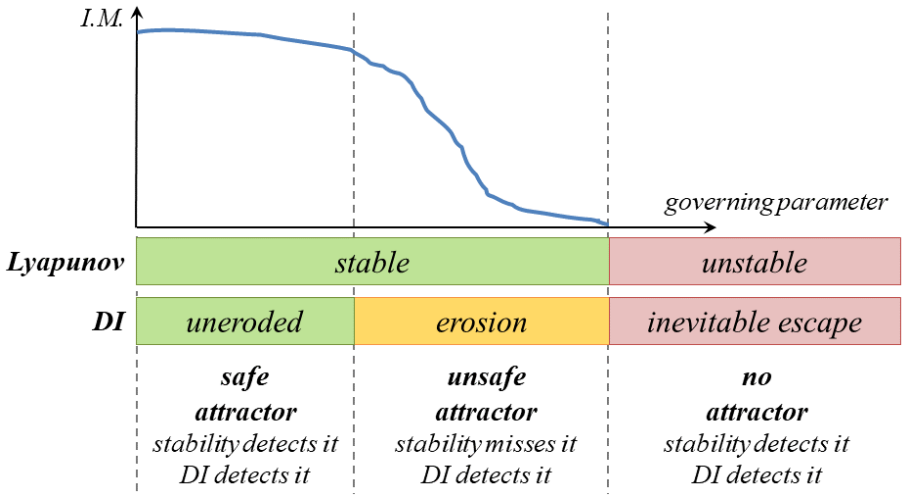

Fig. 10 Schematic of the erosion profile of a potential well in a generic softening system. Local versus global safety assessments [24]. (Colour figure online)

region of intermediate theoretical existence. Here, the local stability analysis of the structure must be *complemented* by a global safety investigation aimed at assessing whether and how safe conditions are actually guaranteed with adequate safety targets. The whole matter will be addressed in more detail forward, in the theoretical vs practical (Sect. 4.1) and engineering design (Sect. 5) perspectives.

For the sake of completeness, it must be noticed that there are also technical situations in which realizing an out-of-well dynamic regime, either 'at infinity' or in an adjacent well, is not dangerous but highly desirable. This is the case of, e.g., a MEMS device to be used as a switch, where the pull-in phenomenon (i.e., the collapse of the device onto the electrically charged substrate) playing the role of escape has to be realized [31]; or of a planar pendulum subjected to vertical harmonic excitation of its support, where the shift from oscillating (in-well) to rotating (out-of-well) dynamics may be of interest for application in wave-energy extraction [32,33].

If systematically constructing integrity/erosion profiles like the one in Fig. 10 for different values of another control parameter (typically, but not necessarily, the excitation frequency), 3D surfaces of dynamical integrity and relevant 2D projections on the excitation parameter plane are drawn. Isointegrity curves (contour lines on the 3D surface) obtained by expressing the erosion profiles in terms of the remaining safe basin percentage (if using the GIM) or, anyway, of the residual DI (if using a different measure), can also be detected. Further on, this kind of DI charts will be seen to play a meaningful role in the practical response and safe design perspective.

DI concepts and tools have been used for assessing system safety of specific mechanical/structural systems since the pioneering studies by Thompson and coauthors in the early 90s, which were mostly focused on the analysis of ship capsizing (see, e.g., [34]), whose possible suppression by means of internally-resonant modal interactions was also highlighted [35]. In the new millennium, extended DI investigations – often also in connection with its possible control (see Sect. 3.3. forward) – have been concerned with archetypal oscillators also describing discrete mechanical models, and with low-order models of continuous structures. The first group refers to the Helmholtz [13] and two-well Duffing [14,27,29] oscillators, the rocking rigid block [36], the parametrically excited pendulum [37], the asymmetrically constrained inverted pendulum [38-40], the shallow von Mises truss [41], the Augusti model [17,42], the guyed pendulum [42,43], a coupled linear oscillator and nonlinear tuned mass damper [44], a nonlinear oscillator excited by non-ideal energy source [45], a truss model liable to snap-through and lateral instability [46]. The second group considers reduced models of structures in macro-mechanics (suspension bridge [47], shallow spherical shell [48], cylindrical shells under different excitations [49-53], general membrane and shell structures [54], composite thin-walled columns [55]), and micro/nano-mechanics (beam-based devices and capacitive accelerometers for MEMS [56-61], micro-plate pressure sensor [62], carbon nanotube [28], noncontact [63-65] and tapping [66] mode atomic force microscopy). In some of the considered systems, the capability of DI analysis to account for the generally detrimental effect of system's imperfections on its overall safety has been shown, too. In more general terms, many other papers have been dealing with stability boundaries of a variety of systems in control space and with the analysis of the evolution of relevant basins of attraction in a safety perspective, however not providing explicit outcomes in terms of DI tools.

3.3 Control of global bifurcations and of dynamical integrity

As discussed in the previous section, the loss of DI, and in particular the safe basin erosion leading to out-of-well dynamics, is triggered by the intersection of the invariant manifolds of a main saddle, usually the hilltop one, governing the system overall dynamics. It is thus quite natural to assume that, whether being able to control the global bifurcation triggering the following integrity reduction, one could also somehow succeed in controlling the latter. In this subsection: (i) The main conceptual features of a control technique aimed at delaying the homo/heteroclinic bifurcation of the governing saddle, shifting it towards higher values of a driving parameter (typically the excitation amplitude), are presented in phenomenological terms; (ii) a summary of control effects on the preservation of a higher dynamical integrity are summarized, distinguishing between different situations of mechanical or dynamical interest. The analytical aspects of the control

technique can be found in [12,15,67,68], and applications to a variety of systems are reported in [13,14,16,27,36,42,43,56,65,69-76], some of them being also concerned with the ensuing integrity outcomes.

Two main aspects of the considered technique are preliminarily pointed out. First, it aims at controlling the overall global dynamics, being different in this respect from other well-established techniques of control of global dynamics or, more specifically, of chaos (like the OGY and the feedback controls, see, e.g., [12]) aimed at stabilizing a specifically desired outcome of the system. Second, such an overall purpose is attained just by exploiting some governing global feature of the underlying dynamics, trying to do it in the best possible way. The technique succeeds in effectively increasing the overall safety of engineering systems in terms of global dynamics.

If fractal basin boundaries occur with the considered harmonic excitation, there is homoclinic intersection, namely the minimum distance (3), rewritten as

$$d = \min_{m\in[0,2\pi]}\{d(m)\} = c\left[1-\frac{\gamma_1}{\gamma^h_{1,cr}(\omega)}\right], \tag{4}$$

by accounting for the expression of the corresponding critical excitation amplitude $\gamma^h_{1,cr}(\omega) = \delta a_0/a_1(\omega)$, with the constant $c = \delta a_0$, is negative for some values of *m*.

As discussed in [12], where references are provided, it is possible to get out from this situation, i.e. to detach the intersecting manifolds, in different ways, namely (i) by increasing the damping, which entails increasing $\gamma^h{}_{1,cr}(\omega)$, (ii) by reducing the excitation amplitude γ_1, (iii) by changing the excitation frequency. All these ways are possibly useful, but they are somehow 'trivial' from the practical viewpoint since they modify the system operating conditions. Other procedures consist of varying the excitation (while keeping its amplitude fixed) in different possible ways, namely by alternatively adding to the reference harmonic excitation (i) external and/or parametric excitations, (ii) subharmonic components entailing a reshape of the excitation and a change of its period, (iii) superharmonic components changing the excitation shape but keeping its period fixed.

In the following, the last procedure is shortly illustrated, since it has been shown to affect quite extensively, and in a favorable way, the preservation of the system's DI, too. Reference is made again to the exemplary Helmholtz oscillator, whose motion equation under a general $2\pi/\omega$-periodic external excitation is modifed as follows:

$$\ddot{x} + \varepsilon\delta x - x + x^2 = \varepsilon\gamma_1 \sum_{J=1}^{\infty} \frac{\gamma_j}{\gamma_1} \sin(j\omega t + \Psi_j) \tag{5}$$

In Eq. (5), $\varepsilon\gamma_1$ represents the amplitude of the basic harmonic, while $\varepsilon\gamma_j$ and Ψ_j are the amplitudes and phases of the controlling superharmonics, to be determined in a possibly optimal way. To better observe the improvements provided by the control technique with respect to the reference harmonic, the excitation in the right-hand side of Eq. (5) is written in terms of the reference excitation amplitude $\varepsilon\gamma_1$, and of the added superharmonic corrections γ_j/γ_1.

The additive expression (2) of the distance between stable and unstable manifolds generalizes to

$$d(m) = \varepsilon\delta a_0 + \varepsilon\gamma_1 a_1(\omega) h(m), \tag{6}$$

where the function

$$h(m) = \sum_{J=1}^{N} \frac{\gamma_j}{\gamma_1} \frac{a_1(j\omega)}{a_1(\omega)} \cos(jm + \Psi_j) = \sum_{j=1}^{N} h_j \cos(jm + \Psi_j), \tag{7}$$

reduces to *cos*(*m*) in the case of harmonic excitation (*j*=1) with assumed zero phase. In turn, the minimum manifolds distance (4) generalizes to

$$d = \min_{m\in[0,2\pi]}\{d(m)\} = c\left[1 - \frac{\gamma_1}{\gamma_{1,cr}^{h}(\omega)}M\right], \tag{8}$$

where the number

$$M = -\min_{m\in[0,2\pi]}\{h(m)\} \tag{9}$$

is positive since $h(m)$ has zero mean value. M does not depend on the reference excitation amplitude $\varepsilon\gamma_1$, which is singled out in (8), while it strongly depends on the shape of $h(m)$ and thus on the shape of the excitation. It summarizes the contribution of the superharmonics added to the reference harmonic excitation (see Eq. (5)). In the case of sole harmonic excitation with zero phase, $M = 1$.

Vanishing of the minimum distance d (Eq. (8)) furnishes the critical excitation amplitude threshold $\gamma_{1,cr}$ for which the homoclinic (or heteroclinic, in more general cases) bifurcation takes place with the considered periodic excitation:

$$\gamma_{1,cr} = \gamma_{1,cr}^{h}\frac{1}{M} = \frac{\delta a_0}{a_1(\omega)}\frac{1}{M}. \tag{10}$$

Note that the simple expression (10) ensues from the linear nature of the distance with respect to γ_1 and does not hold in general. For instance, when the manifolds distance is computed numerically [65,72], the solution of $d = 0$ requires solving a nonlinear algebraic equation. However, $\gamma_{1,cr}$ is a function of all the other system parameters, independent of whether it is computed exactly, as in piece-wise linear systems [16,67], by a perturbative approach, as in (10), or numerically. It is also worth stressing that the shape of the excitation affects Eq. (10) only through the number M, which accounts for the effects of the added superharmonics. In other cases, the dependence of $\gamma_{1,cr}$ on the excitation shape is expected to be more involved.

Both the minimum distance d (Eq. 8) and the homoclinic bifurcation threshold $\gamma_{1,cr}$ (Eq. 10) are inversely proportional to the shape parameter M; accordingly, control is realized by decreasing M. Two different perspectives can be assumed. One aims at avoiding intersection of stable and unstable manifolds, thus modifying their currently negative minimum distance to positive. In this case, the underlying global bifurcation event is not explicitly involved in the analysis, and the interest is towards attaining a 'local' dynamical outcome for assigned system parameters and operational conditions. A different control perspective pays attention to the 'overall' system behaviour, thus being of greater relevance from an engineering viewpoint. It consists of implementing the control in such a way to shift, e.g., the homoclinic (or heteroclinic) bifurcation threshold in the excitation parameters space towards higher amplitudes. Here, the focus is on the global bifurcation threshold as a whole. Focusing on this latter, more general, perspective, the overall critical thresholds of the Helmholtz oscillator in parameters space, obtained with either the reference harmonic excitation (uncontrolled system) or a periodic excitation also including superharmonic components (controlled system), are shown in Fig. 11. It can be seen how, by properly assuming h_j and Ψ_j in Eq. (7), it may be possible to get M values lower than the unity in Eq. (10) and such to rise up the critical threshold $\gamma_{1,cr}$ (when also including superharmonics) with respect to the critical threshold $\gamma_{1,cr}^{h}$ (with the sole harmonic excitation). For the former (controlled) system, the extent of the region without homoclinic intersection (below the corresponding threshold) is increased with respect to that of the latter (uncontrolled) system, with a saved region being realized in optimal way via the control application. The improvement against homoclinic bifurcation can be quantified by the gain

$$G = \frac{\gamma_{1,cr}}{\gamma_{1,cr}^{h}} = \frac{1}{M}. \tag{11}$$

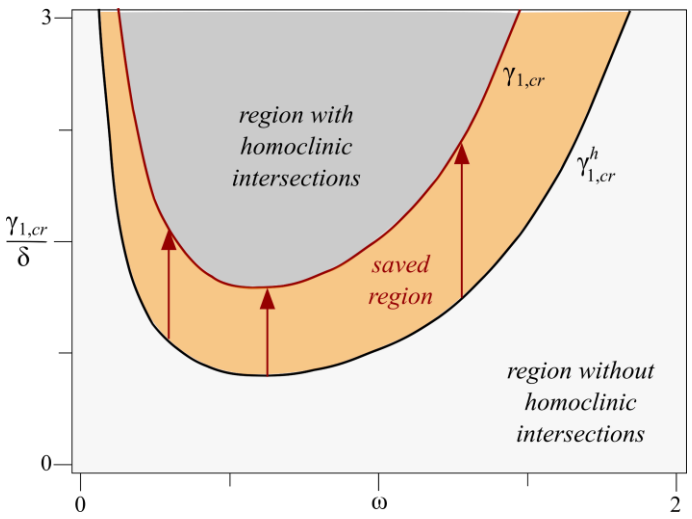

Fig. 11 Helmholtz oscillator: the optimal saved region [12]. (Colour figure online)

The above qualitative concepts have been successfully implemented in a general control technique, whose involved analytical and operational details can be found in [15,67,68]. Its main features are summarized as follows.

- If the manifolds involved in the homoclinic (heteroclinic) bifurcation pertain to a hilltop saddle (two different hilltop saddles), the relevant critical thresholds can be detected analitically through the Melnikov perturbation method.
- The optimal mathematical choice of h_j and Ψ_j in Eq. (7) allows to detect controlling superharmonics γ_j which maximize the theoretical gain, i.e. to identify the optimal $2\pi/\omega$-periodic excitation.
- The optimal theoretical values of h_j (with Ψ_j =0) are system-independent, namely the control method is 'universal'; however, its practical implementation is system-dependent, since the amplitudes $\gamma_j(h_j)$ of the controlling superharmonics change from system to system.
- Depending on the governing global mechanisms, two main different strategies can be implemented: (i) one-side (or topologically localized) control, in which only one global bifurcation is controlled, as it occurs typically in systems with one potential well; (ii) global (or topologically spread) control, in which more global bifurcations are simultaneously controlled, as it may occur in multiwell systems.
- Practical applications of the different control strategies often succeed in satisfactorily (though non-optimally) shifting the critical bifurcation threshold of interest towards higher excitation amplitudes even when adding to the reference harmonic excitation only one optimal superharmonic, for which it may technically make sense to require a relatively low 'cost' in terms of added resources (i.e., in general, $|\gamma_j| < |\gamma_1|$).

If the saddle manifolds actually triggering the safe basin erosion are correctly detected, the control technique always succeeds in shifting *also* the (sharp) fall down of a generic integrity profile (see Fig. 10) towards higher excitation amplitudes, thus improving the system overall robustness and safety, to a variable extent. Instead, in general, the global bifurcation control has no meaningful consequences on the system final (inevitable) escape, which would indeed go well beyond theoretical expectations about its possible effects.

Jointly looking at both DI analysis and its overall control with the global bifurcation technique, the outcomes of a number of papers published in the first decade of the new millennium have been summarized in [12,36]. They are classified according to various criteria paying attention to the mechanical, dynamical, bifurcation and control features of archetypal oscillators describing the physical behaviour of real systems in engineering science and mechanics, and being used in a cross-correlated perspective. Mechanical systems are categorized according to their (i) being smooth or non-smooth, (ii) having single- or multi-well potentials, (iii)

exhibiting softening or hardening behaviour. Dynamical aspects are distinguished according to the system (iv) having symmetric or asymmetric characteristics, (v) being resonant or non-resonant, and the operating conditions of interest being (vi) mostly steady or also transient. Bifurcation and control aspects are classified as (vii) involving homoclinic or heteroclinic manifolds, (viii) dealing with overall or local bifurcation control, (ix) entailing approximate or exact bifurcation analysis, (x) possibly implementing a mixed (analytical-numerical) control strategy or necessarily relying on a purely numerical one.

In the very last decade, further investigations on DI and its overall control have been conducted in the more clearly focused and aware perspective of improving system safety [77], by considering reduced models describing the low-order nonlinear dynamics of either structures liable to unstable interactive buckling of interest in macro-mechanical applications [78], or cantilevered structures used in micro/nano-systems [79].

Focusing on the erosion/escape issue, a summary schematic flowchart of the system's dynamical integrity scenario and its global bifurcation control is shown in Fig. 12. Considering escape to either infinity or an adjacent well, and distinguishing between its being unwanted, as in most technical applications, or wanted, as it sometimes occurs also in the mechanical context, the possibility to control (i.e. delay) or anticontrol (i.e. accelerate) (e.g., [74]) the erosion phenomenon leading to escape via the global bifurcation control is highlighted.

To summarize, DI-based analysis and control of a given system, to be used also for design purposes, involves the following operational steps.

(i) Identifying the safe basin whose steady dynamics has to be guaranteed.

(ii) Selecting and comparatively evaluating integrity measures accounting for the safe basin width and/or compactness.

(iii) Costructing and comparing integrity profiles providing the evolution of the safe basin robustness with a main varying control parameter, along with overall 2D charts highlighting the residual integrity in (usually excitation) parameters space, to be used for overall addressing possible discrepancies between theoretical and practical stability, and to get hints about possibly novel design criteria.

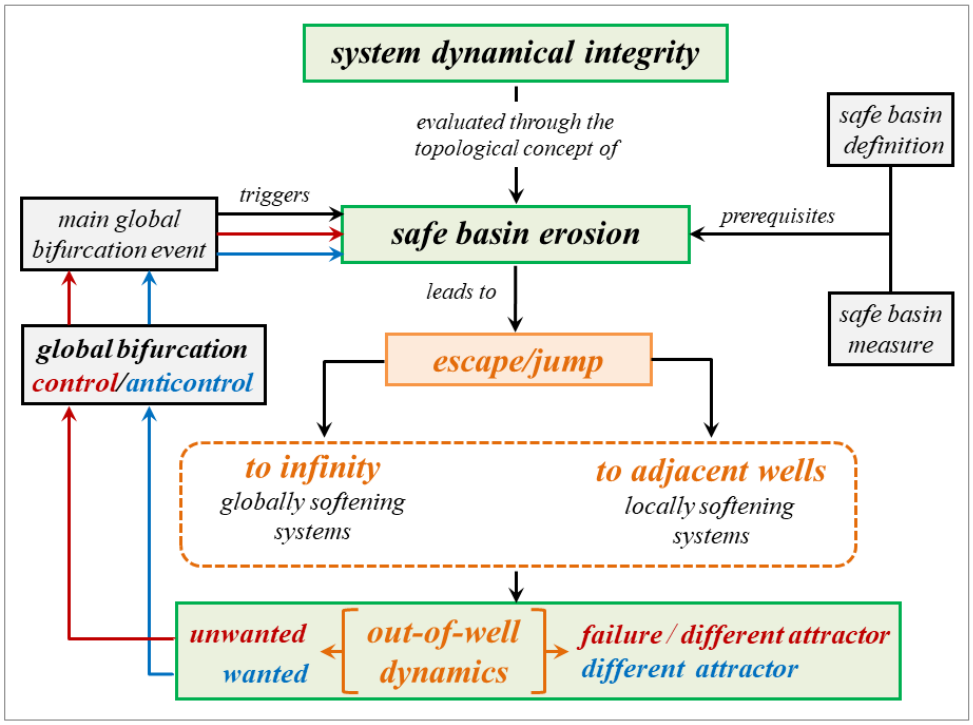

Fig. 12 Dynamical integrity (erosion) scenario and its control. (Colour figure online)

(iv) In different parameter ranges of interest, detecting the saddle, among the many exhibited by the system, whose invariant manifolds tangency triggers the fractal dynamics (later on) entailing a possibly sharp and dangerous fall down (erosion) of the integrity profile.

(v) In different parameter ranges, implementing a 'sub-optimal' control procedure of the homo/heteroclinic intersection of the detected saddle(s) manifolds, able to shift it towards higher values of the varying control parameter, with beneficial effects also in terms of delay of the (possibly sharp) basin erosion and preservation of an acceptable residual integrity.

In Sect. 4 forward, a noncontact AFM will be considered as an illustrative system of interest in micro-mechanics for highlighting (i) the features of a DI analysis aimed at evaluating the system safety in different operating conditions, and (ii) the capability of the global bifurcation control to enhance the robustness of desired dynamical outcomes.

Overall, exploiting an important global property of a system – the intersection between stable and unstable manifolds of a saddle – when varying a driving parameter, allows:

- to control the homo/heteroclinic bifurcation which triggers erosion;
- to suitably increase the system robustness in parameters space in terms of desired operational conditions.

Further DI issues will be dealt with in Sect. 5, (i) discussing the role that theoretical/numerical evaluation of dynamical integrity may play for interpreting experimental results and predicting some relevant outcomes, and (ii) generally dwelling on the contribution that DI analysis and control may furnish for a novel and enhanced, yet aware, design of engineering systems and structures, also possibly accounting for the uncertainty quantification issue.

3.4 Basin stability: a purely computational approach to global dynamics

Due to multistability, detecting all possible coexisting solutions and basins of attraction (including the very small ones of rare attractors [80]) is quite complicated already in single-dof systems. For multi-dof systems, this becomes nearly practically impossible, mostly if the initial conditions cannot be precisely predicted and a wide range of system parameters has to be analyzed. To overcome these issues, the basin stability (BS) method [81] using Bernoulli trials to estimate the volume of a basin of attraction has been proposed, along with other tools for the analysis of multistable systems based on survivability [82] and basin entropy [83] concepts. The former includes the analysis of transient motions, the latter aims at quantifying uncertainties and getting information about the structure and compactness of basins of attraction.

In the BS method, motion equations are integrated N times for randomly chosen initial conditions, different in each trial, and the analysis of the relevant outcomes allows to evaluate the stability of each solution. If only one solution exists, all trials give the same result, but if more attractors coexist, the probability of their occurrence, which represents a stability measure of corresponding basins, can be estimated for a chosen set of initial conditions. The obtained basin volume is similar to the global integrity measure (GIM) of the DI analysis. However, the necessarily low attention paid in the BS method (in the multi-dof perspective) to identifying, describing and visualizing the bifurcational and topological aspects behind instability phenomena entails low information about the actual compactness of the safe basin of a desired dynamical outcome (not necessarily an attractor), which strongly affects its robustness.

In the classical BS approach [81] the values of system's parameters are assumed to be fixed. However, a mechanical/structural solution of practical interest has to be stable and with a dominant basin of attraction in a given (accessible) range of system parameters. Thus, in the extended BS method [84] some selected parameters are chosen randomly, too, and N trials of numerical simulations allow to estimate the probability $p(A)$ that the system will reach a given attractor A of interest, with the precise description of other coexisting attractors being not necessary. The underlying idea is that system parameters are measured or estimated with a finite and not always achievable accuracy, and that their values can vary during normal operation. Therefore, modifying parameter values allows to describe how some relevant mismatch or model imperfections influence the system dynamics and entail a risk of failure associated with the presence of coexisting attractors. The BS

approach has been successfully used to detect and classify coexisting solutions in a number of multistable, mostly two-dof, mechanical systems [85,86], with also experimental verification [85]; a relevant summary is reported in a recent review paper [87].

Two-parameter maps of basin stability, and corresponding 2D probability density plots, can be constructed for a number of competing solutions. The former allow to get absolute measures of the probability (i.e., basin volumes in different parameter ranges) that, notwithstanding the random perturbation of a parameter, the system will end up in the relevant basins of attractions, thus detecting a possibly dominant basin with relatively high stability measure nearly everywhere, which corresponds to low susceptibility to perturbations. In turn, the latter enable to detect where the basin of a given attractor has the biggest relative volume (i.e. the highest relative probability), which allows to analyse changes in the volume itself. Overall, ranges in parameter space in which the solution is the most likely to appear and has low susceptibility to perturbations can be detected. In this respect, the BS method is certainly more effective than classical analyses of nonlinear systems through path-following, numerical integration, and basins of attraction, even though its outcomes should be suitably paralleled by classical ones concerned with the structure of solutions, mostly if the system has multiple attractors or the basins of attraction are especially complex.

Sample based analysis of the BS method may also help getting information on the phase space organization, which is substantially unknown in multi-dof systems due to the computational challenge needed to build basins of attraction. This is realized by analysing how the probability to reach a given attractor varies when varying one or two generalized coordinates. 1D probability histograms with one varying initial coordinate may indicate not only minimum or maximum volume of the basin of attraction of a given solution but also changes in its structure and volume. Indeed, large dispersion along the histogram indicates fractal structure of the basin, whereas a clearly visible trend corresponds to a more compact shape. 2D density plots in phase space show how the probability to reach a certain solution changes with respect to two particular coordinates, thus bringing more information. These are of interest mostly for mechanical systems, where they reflect the influence of varying initial displacement and velocity of a given dof. Thus, 2D density plots can be effectively used to investigate the structure of the phase space in multidimensional systems. Overall, particular features of the phase space topology are obtained, along with some hints about basins compactness.

One further extension of the sample based analysis is just concerned with the phase space structure, by taking into account its time evolution in such a way to characterize the time-dependent susceptibility to perturbations of the initial conditions along a stable periodic trajectory [88]. Different measures can be used to quantify the closeness of a trajectory to the stability margin within one full period of motion, the more natural one being the minimum Euclidean distance in phase space between the current position on the attractor and the boundary of its basin of attraction. This is just the local integrity measure (LIM) of the DI approach (see Sect. 3.2), here, however, meaningfully considered in its time evolution, because a given perturbation may or may not lead to the adjacent boundary of the basin of attraction mainly depending on when it occurs. Indeed, analysis of changes in the minimum distance allow to identify crucial parts of the stable trajectory closest to the adjacent boundary, where even small perturbations can induce the sudden, and possibly dangerous, switch to another solution. In the case of fractal basins, a sufficient number of Bernouilli trials performed in a given interval of the considered trajectory will highlight a minimal distance from the basin boundary which goes to zero. Thus, the method can be used to identify attractors with fractal basins, somehow expanding the knowledge about the overall structure and compactness of the phase space.

4 Dynamical integrity for analysis and control: a noncontact AFM

Motion control of nonlinear mechanical structures and systems has been investigated in-depth in the last two decades, with the aim of improving the system dynamical performances by avoiding possible unstable or chaotic responses. This is particularly important for micro/nano mechanical systems, in which slight changes of the initial system operating parameters and/or initial position and velocity can cause strong alterations of the dynamical response, leading to possible unstable, aperiodic, and chaotic oscillations, which represent

undesirable behaviours entailing a restriction of the operating range. Among them, Atomic Force Microscopes (AFMs) working in noncontact mode can display an instability of the equilibrium configuration called 'jump-to-contact' (or escape, in dynamical systems terms), which occurs when the atomic attraction between the tip of the cantilever and the sample to be scanned overcomes the restoring elastic force of the beam. Such condition induces contacts between tip and sample, which cause errors in the topography process. To avoid failure of the device operations, several control methods have been applied to AFMs, mostly based on feedback control techniques.

4.1 Highlighting unsafe overall dynamics under feedback control

As archetype of control technique tailored to improving the local dynamics, a simple external feedback control is applied to the continuum formulation of a noncontact AFM model, in order to keep the microcantilever motion close to an appropriate reference response, corresponding to the solution of the relevant uncontrolled system under the same set of parameters values [89]. The single-mode reduced equations are

$$\ddot{x} + \alpha_1 x + \alpha_3 x^3 = -\frac{\Gamma_1}{(1 + x + z - z_s)^2} - \rho_1 \dot{x} + x\mu_1 \omega^2 U sin(\omega t) \tag{12a}$$

$$\dot{z} = k_g (x_{ref} - x) \tag{12b}$$

where $x(t)$ is the transverse displacement of the microcantilever tip; $z(t)$ is the control variable which represents the distance between the clamped part of the microcantilever and the horizontal reference axis; z_s is the displacement of the sample with respect to the selected reference position; k_g is the external feedback control parameter; α_1 and α_3 are linear and cubic stiffness coefficients, respectively; ρ_1 is the linear damping coefficient; Γ_1 is the attractive atomic interaction coefficient; ω and U are frequency and amplitude of the horizontal parametric scan excitation, and $x_{ref}(t)$ is the periodic reference response of the uncontrolled system (Fig.13a). It is worth specifying that the control works when the response $x(t)$ settles onto $x_{ref}(t)$, i.e., when z coincides with the expected value z_s (Fig.13b). The herein presented analyses have been developed for the following set of parameter values: $\alpha_1 = 1,\ \alpha_3 = 0.1, \rho_1 = 0.001, \Gamma_1 = 0.1, \mu_1 = 1.5708, k_g = 0.001, z_s = 0.01$, for which the corresponding natural frequency is $\omega = 0.8358$.

Due to the local nature of the applied feedback control procedure, aimed at stabilizing single suitable responses, it is of interest to verify and discuss its effect on the system overall dynamics, which is generally unknown. Numerical analyses of system (12) have been accomplished to evaluate the influence of several system parameters, which include excitation frequency and amplitude, nonlinear atomic interaction, and feedback control parameter [90]. The detected bifurcation scenario of the controlled system displays a rich behaviour characterized by the occurrence of torus and transcritical bifurcations, absent in the dynamics of the uncontrolled model [63], which involve the system periodic responses and induce an apparent reduction of the stability boundary. Figure 14 shows the behaviour chart in the frequency–amplitude plane where the overall

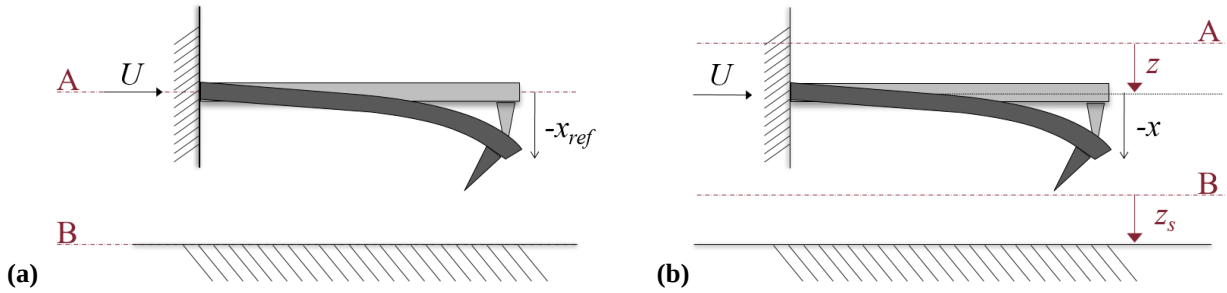

Fig. 13 AFM microcantilever in the reference configuration **(a)** and in a generic position **(b)**; A and B lines represent the reference positions of microcantilever and sample surface, respectively.

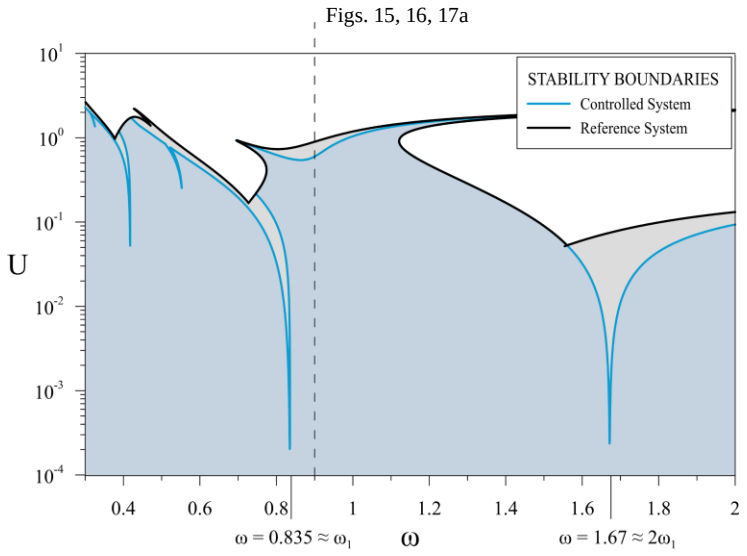

Fig. 14 Stability chart in the ω-U plane with representation of the overall escape thresholds for the controlled (k_g=0.001, blue line) and reference (k_g =0, black line) systems. Cyan area: stability region of the controlled and reference systems; gray area: stability region of the sole reference system. (Colour figure online)

escape thresholds of the controlled (blue) and uncontrolled (black) systems are compared, and the corresponding stability regions are detected. In a close neighborhood of the main resonance frequencies, the feedback control produces instability tongues responsible for a strong decrease of the amplitude value corresponding to escape. Such tongues are generated by the inability of the feedback control of dominating the resonant periodic responses, whose amplitude increases significantly in the resonance regions. As a consequence, the sole non-resonant responses, which around resonance become unstable for low values of the forcing amplitude, govern the escape threshold of the controlled system.

Besides these analyses aimed at verifying the effect of feedback control as a function of system parameter variation, changes in the system initial conditions possibly due to imperfections must be considered. In fact, the topography of noncontact AFMs is crucially associated with the tip-sample distance, which can be sensibly modified by slight changes in the initial position and/or velocity. Consequently, the overall performance of the local feedback control has to be assessed, too, via the investigation of the system dynamical integrity, i.e., the detection of the basins of attraction of the main system responses, together with the analysis and quantification of how the relevant erosion processes do evolve [64].

The investigation of the DI under variation of some control parameter is strictly connected with the definition of safe basin, which represents the union, in phase space, of all initial conditions assuring selected response performances. From what previously said, for the AFM system with external feedback control the safe basin must include only the solutions on which the control procedure correctly works, thus excluding, e.g., the resonant responses around resonance frequencies which the control cannot correctly manage. Conversely, for the reference (uncontrolled) system, the safe basin coincides with the single potential well characterizing the Hamiltonian dynamics, which includes all basins of the bounded responses.

From Eqs. (12), to be completed with the ODE describing the dynamics of the reference system x_{ref}, the controlled system results to be five-dimensional in the state space, and the relevant attractor–basin portraits are quite difficult to represent and interpret. Therefore, to achieve understandable results, analyses are performed by systematically assuming that the initial displacement and velocity of the controlled system are those of the reference one, i.e., $x(0) = x_{ref}(0)$, $\dot{x}(0) = \dot{x}_{ref}(0)$—which also corresponds to situations in which the control is more likely to operate—, thus reducing the study to three-dimensional basins. The erosion evolution is hence investigated by fixing trivial initial condition of the control variable z, in order to construct 2D cross-sections of the basins of attraction by means of an ad hoc routine.

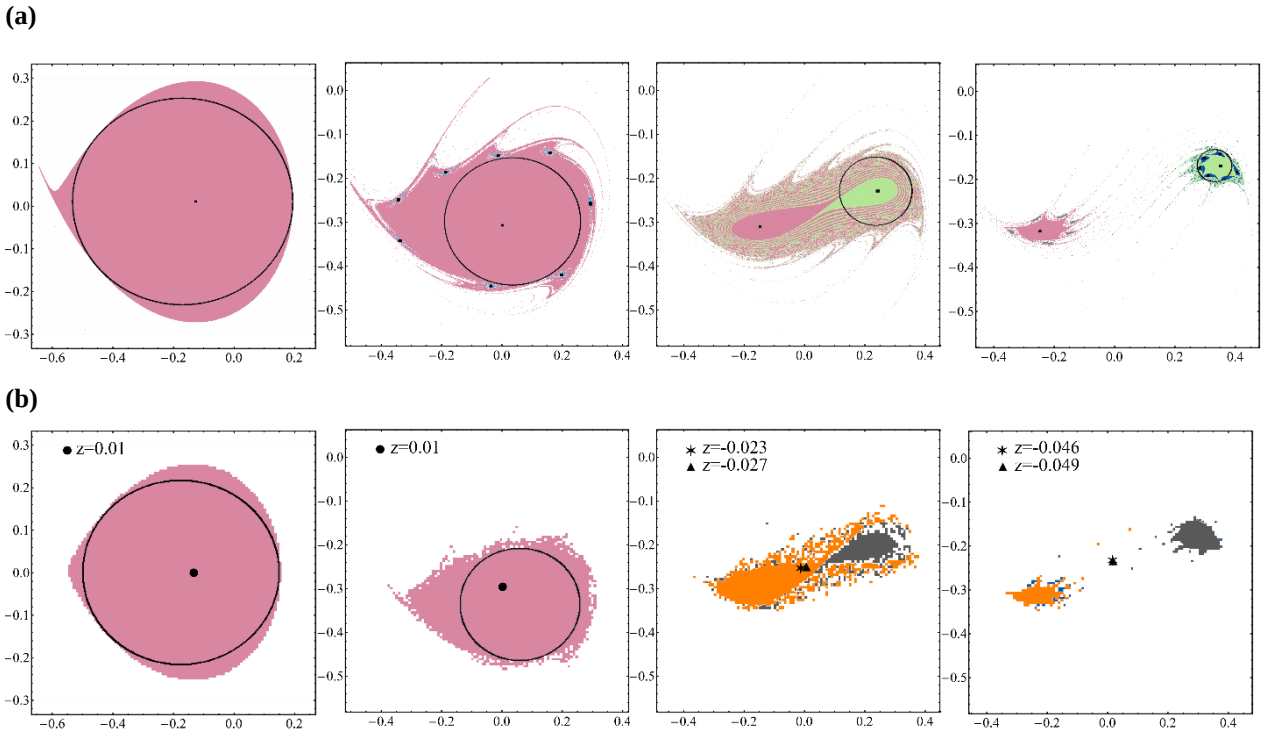

Fig. 15 Attractor-basin phase portraits in the $(x, \dot{x})$ plane at $\omega = 0.9$ and $U = 0$, $U = 0.5$, $U = 0.65$, $U = 0.75$, for the reference system **(a)**; cross-sections in the $(x, \dot{x})$ plane of the basins of attraction for the system with feedback control **(b)**. The black circle represents the IF measure of the safe basin. (Colour figure online)

Figure 15 shows the basins of attraction evolution for increasing forcing amplitude after the resonance frequency, i.e., $\omega = 0.9$ (see Fig. 14), comparing the outcomes of the controlled and uncontrolled models. Looking at the behaviour of the reference system (Fig. 15a), the response is governed by the purple 1-period solution occupying the whole potential well, which is eroded, as the amplitude increases, by the white basin of the unbounded solution penetrating inside the well, with very small basins of multiple period solutions also growing up at the purple basin edge in narrow ranges of forcing amplitude. For high values of the latter, a second 1-period solution (green) arises inside the well, whose development occurs to the detriment of the existing basin, up to splitting in two separate basins before being completely eroded by the unbounded basin (third and fourth portraits of Fig. 15a).

Starting from this situation, the presence of the external feedback control produces an increase of the safe basin erosion caused by the enlargement of the surrounding basin of unbounded solution, with the disappearance of high period solutions at the purple basin edge. More importantly, the feedback control is capable to correctly reproduce the targeted 1-period solution only in a defined range of the harmonic excitation amplitude, above which the periodic responses exhibited by the system can no longer be considered acceptable. This is due to the onset of a new transcritical bifurcation in the controlled system, which unstabilizes the purple 1-period solution at $U = 0.598$, thus representing the applicability limit for the feedback control. Above this value, in fact, the two stable periodic solutions displayed by the controlled system (which are indeed represented by basins of different colours in the last two portraits of Fig. 15b) do not coincide with the reference solution. This is shown in the phase portraits of Fig. 16, where the mechanical responses in both the right (green/gray) and left (purple/orange) basins are different for the systems with and without control (Fig. 16a) and $z \neq z_s = 0.01$ (Fig. 16b), highlighting the bad control operation.

To quantify the overall erosion process, the Global Integrity Measure (GIM) and the Integrity Factor (IF), respectively including and neglecting the basins fractal parts, are employed to build the integrity profiles of the safe basin for different forcing frequencies, those at $\omega = 0.9$ being reported in Fig. 17a by way of example.

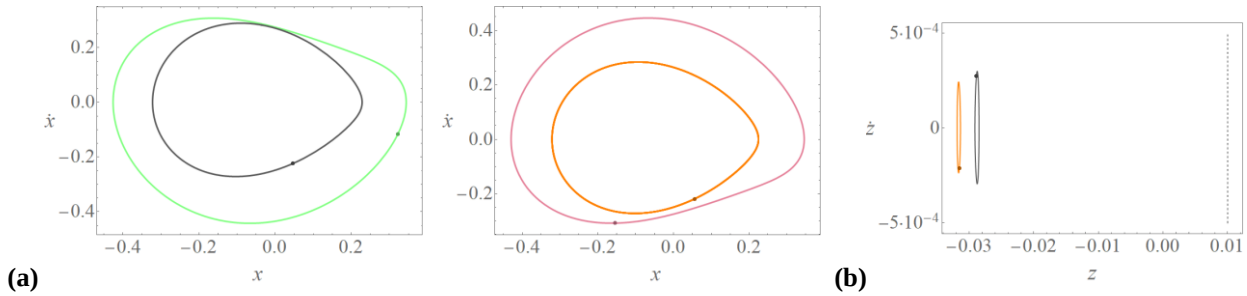

(a) **(b)**

Fig. 16 Phase portraits of the two 1-period solutions in the mechanical **(a)** and control **(b)** planes, at $\omega = 0.9$ and $U = 0.7$, for the reference system (green/purple) and for the system with feedback control (gray/orange). i.c. $(x, \dot{x}, z)(0) = (0.2, -0.2, 0), (-0.2, -0.3, 0)$. Solutions colours correspond to basins of Fig. 15. (Colour figure online)

The results are summarized in Fig. 17b, which shows different iso-integrity curves, i.e., frequency-dependent thresholds characterized by a constant level of residual integrity actually governing the practical safety, for the system with (blue) and without (black) control. In Fig. 17a, the limit value $U = 0.598$, responsible for unstabilization of the controlled solution, produces the downfall of the profiles from 50 to 0%, which reflects on the evident packing of the corresponding iso-GIM curves of Fig. 17b and underlines the unreliability of the feedback control when the system works around these high-amplitude values. Note that this occurs at a frequency value $\omega = 0.9$ somehow shifted from the most pathological range of resonance where, at $\omega = 0.8$, an even more dramatic shift of the feedback erosion profiles towards lower excitation amplitudes does occur, with respect to the uncontrolled ones [64,79]. Indeed, the overall worsening of system practical stability in Fig. 17b due to the presence of control is especially meaningful around the natural resonance frequency, with also a shift in the lowest peak of each curve, which moves from the nonlinear resonance frequency to the natural one. This is due to the system softening behaviour which, in that range, avoids the response from achieving the resonant solution of high amplitude, whose residual integrity is too scarce.

From a practical viewpoint, it is worth noting that the suppression of the bistable region of resonant/nonresonant responses, and in general a reduction of multistability, can be interpreted as a positive effect of control, as it prevents possible unexpected transitions from low-amplitude to high-amplitude responses potentially responsible for distortions in the scanning operations of the sample. However, this positive effect is nullified by the onset of instability tongues in the resonance regions, which exhibit an even more dangerous scenario from an operational perspective, and the concurrent penetration of the unbounded basin inside the potential well causes a strong reduction of the system safety for very low parameter values.

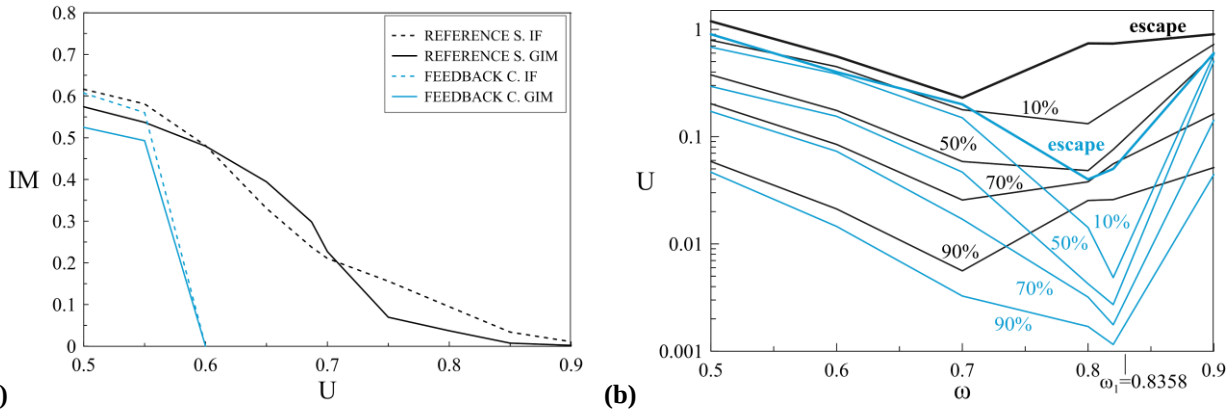

(a) **(b)**

Fig. 17 Enlargement of the final part of the erosion profiles at $\omega = 0.9$ for the controlled (blue) and for the reference (black) systems **(a)**; residual iso-integrity curves of the safe basin **(b)**. (Colour figure online)

4.2 Enhancing dynamical robustness via global bifurcation control

Beyond the local feedback control considered in the previous section, the globally oriented control presented in Sect. 3.3 is applied here to the AFM system, with the objective of exploiting its global dynamical properties to reduce the erosion of the safe basin responsible for the loss of safety, thus preserving the system DI. The goal of the method is to delay the occurrence of the global events which trigger the erosion, represented by the homoclinic or heteroclinic bifurcation of some saddle of the system, by means of the optimal modification of the excitation shape. As a consequence, the system dynamics is overall controlled and the safe region is enlarged in parameter space. Accordingly, the harmonic excitation of the AFM model is modified by the addition of controlling superharmonics of amplitudes U_j and phases Ψ_j, (j = 2,n),:

$$\ddot{x} + \alpha_1 x + \alpha_3 x^3 = -\frac{\Gamma_1}{(1+x)^2} - \rho_1 \dot{x} + x\mu_1 \omega^2 U_1 \sum_{j=1}^{n} \frac{U_j}{U_1} sin(j\omega t + \Psi_j), \tag{13}$$

where U_1 represents the harmonic forcing amplitude.

In order to define amplitudes and phases of the optimal controlling superharmonics, the crucial step is represented by the identification of the global bifurcation triggering erosion. In fact, when it involves the manifolds of the sole hilltop saddle, its (approximate) occurrence can be determined by means of the asymptotic Melnikov method, and the shape of the optimal controlling superharmonics can be analytically detected. However, when the hilltop saddle bifurcation occurs at amplitudes much lower than those associated with the initial decrease of system safety, i.e. with the fall down of the safe basin erosion profile, its control does not work [79,91]. In such cases, the global event to be controlled must be sought among other bifurcations related to the manifolds of internal saddles, which exist when several basins are competing inside the potential well. Unluckily, the analytical control method cannot be applied to these bifurcations, and a purely numerical procedure is required.

Focusing on the same frequency value $\omega = 0.9$ of the previous section, and paying attention to the sharper final part of the integrity profile of the reference system (black curves in Fig. 17a), which marks the loss of safety, a careful investigation of its global behaviour allows to identify an internal saddle S_1 appearing at a quite large value of the excitation amplitude (U = 0.604), due to the birth of the basin of a new competing 1-period solution [79]. As the amplitude slightly increases, at $U \cong 0.686$ (see Fig. 18b), a homoclinic bifurcation involving the left manifolds $W_l^u(S_1)$ and $W_l^s(S_1)$ of the S_1 saddle occurs and, from a phenomenological point of view, the basins start separating inside the potential well, causing a considerable reduction of the system dynamical integrity.

In order to control such homoclinic bifurcation, it is worth noting that, for high values of the excitation amplitude, the local organization of the in-well basins of attractions is topologically similar to that of a symmetric two-well potential (see the third portrait in Fig. 15a, and also Fig. 18a for convenience), notwithstanding the AFM system displays an overall asymmetric one-well potential. To optimally control it,

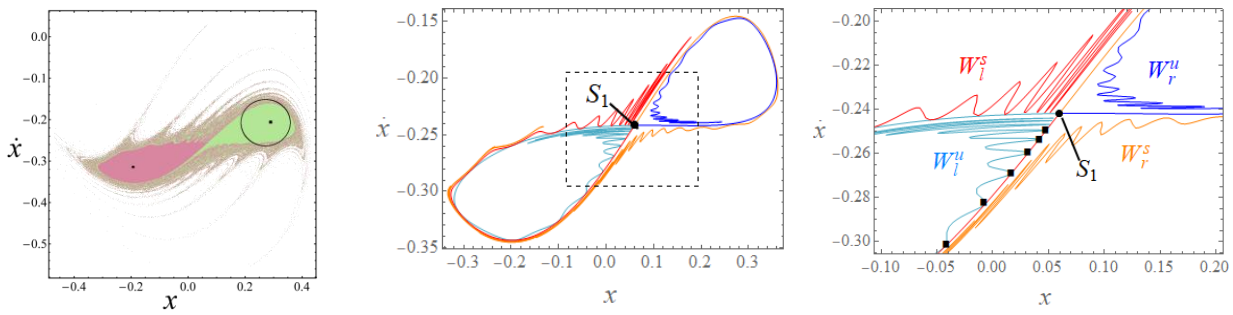

(a) **(b)**

Fig. 18 Reference system. Basins of attraction and manifolds (large view and zoom) at $\omega = 0.9$, for $U = 0.686$. Orange (blue) line: stable (unstable) right manifold of S_1 saddle; red (cyan) line: stable (unstable) left manifold of S_1 saddle; square dots: bifurcation points. (Colour figure online)

addition of odd superharmonics is required (the so-called 'global' or 'two-side' control), instead of the 'one-side' control with even superharmonics (see, e.g. [15]) which would be generally applied for the AFM model [65]. Consequently, one odd superharmonic ($j = 3$) is introduced in addition to the harmonic forcing, and its optimal shape is determined by means of an entirely numerical procedure, assuming $\Psi_j = 0$ to lighten the onerous numerical effort. After having detected a suitable region in the phase plane including graphically convenient bifurcation points (squared points in the enlargement of Fig. 18b), the evaluation of the manifolds distance along a suitable (i.e., nonparallel to one of the manifolds) direction is performed by means of the arclength method. To this aim, one manifold is numerically discretized and the distance from each of its points to the other manifold is calculated in order to identify the minimum value. The process is serially applied with different values of the harmonic amplitude U_1, up to the zeroing of the minimum computed distance, that is the manifolds tangency, which corresponds to the occurrence of the global bifurcation. Repeating the procedure with several values of the superharmonic amplitude, namely different U_3/U_1 ratios in Eq. (13) (see Fig. 19a), allows to obtain the threshold of the homoclinic bifurcation, whose peak occurs for $U_3/U_1 = -0.45$, which represents the not too 'expensive' optimal amplitude of the controlling superharmonic to be adopted. The impact of the optimal controlling superharmonic on the basins organization can be observed by comparing the phase planes of the reference system in Fig. 18 with those of the controlled one in Fig. 19b. The birth of the competing 1-period response (green basin) is significantly delayed to higher amplitude values, as well as the basins' separation inside the potential well, thus increasing the robustness of the dominant (purple) basin. Moreover, the evolution of both the left and right manifolds of the internal saddle S_1 is evidently smoother, proving the effectiveness of the 'two-side' control in governing the organization of both wells, or basins as in the present case, ruled by the detected saddle.

Figure 20a shows the comparison between the erosion profiles of the reference system (black) and of the system with optimal superharmonic (red), and highlights the ability of the global control in increasing the amplitude range which ensures the system safety by shifting the fall down of the safe basin profile to higher U

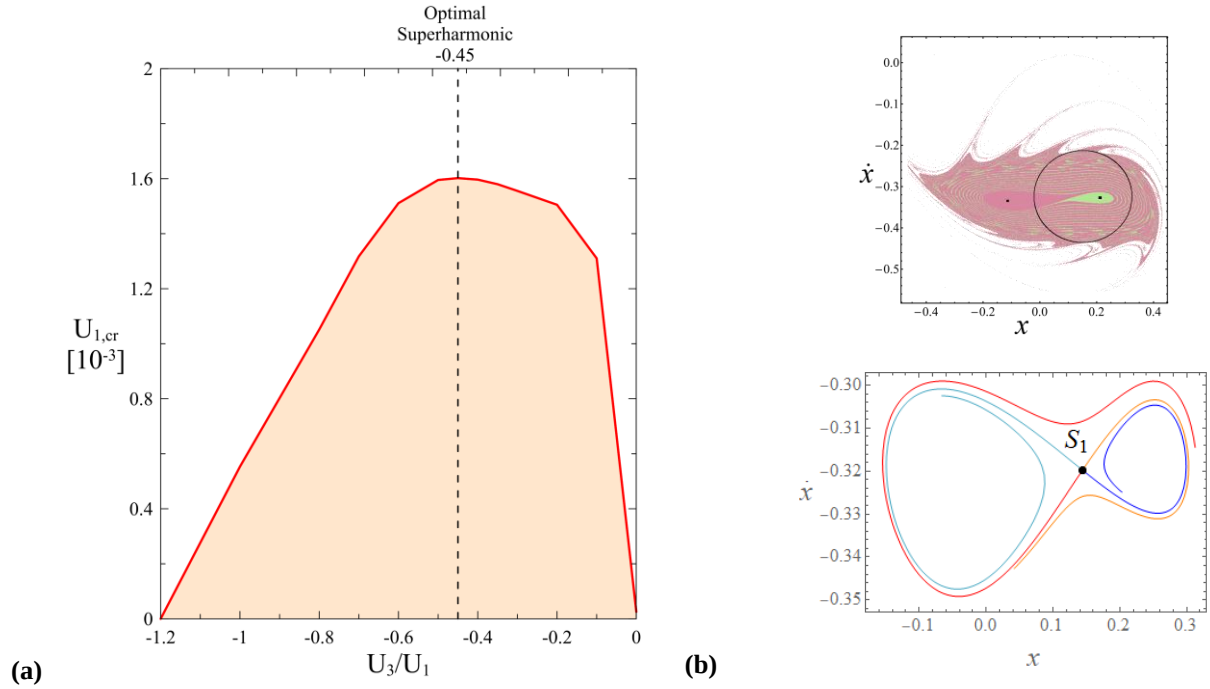

Fig. 19 Numerical threshold of the homoclinic bifurcation $W_l^u(S_1) \cap W_l^s(S_1)$ as a function of the superharmonic amplitude U_3/U_1 **(a)**; basins and manifolds for the system with optimal superharmonic $U_3/U_1 = -0.45$, for $U = 0.686$ **(b)**. (Colour figure online)

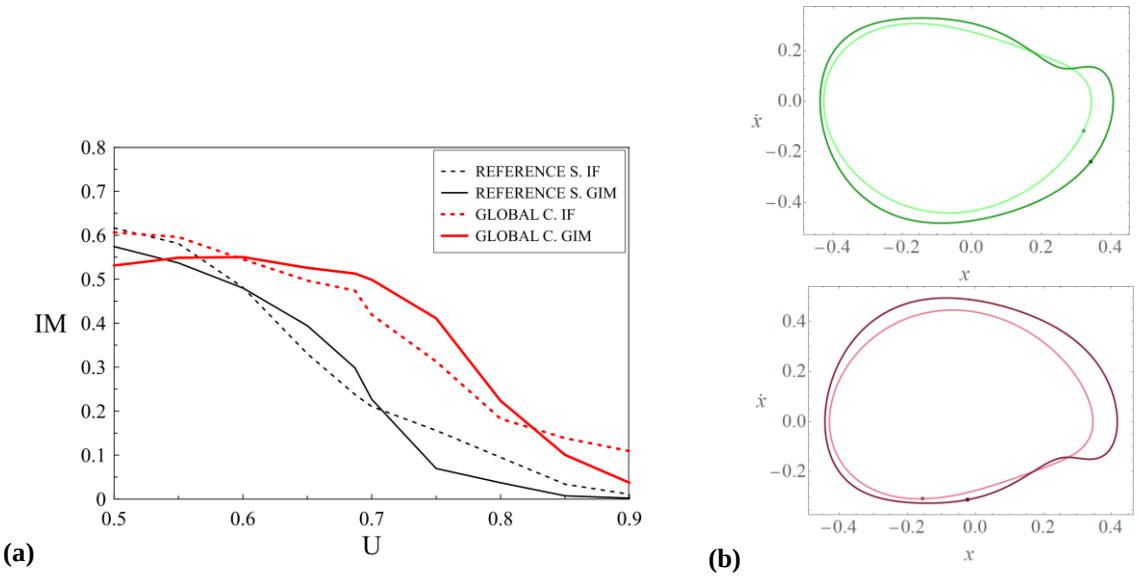

Fig. 20 Enlargement of the final part of the erosion profiles at $\omega = 0.9$ for the reference system (black) and for the system with optimal superharmonic $U_3/U_1 = -0.45$ (red) **(a)**; Periodic solutions in the state plane at $U = 0.7$, for the reference system (green/purple), and for the system with optimal superharmonic (dark green/dark purple) **(b)**. (Colour figure online)

values. Concurrently, the overall trend of the erosion profiles remains essentially unaltered, while just slight changes of amplitude and shape occur in the system response (see Fig. 20b).

As a final comment, it is worth discussing the effects on the system robustness and safety against jump-to-contact of the two analyzed control techniques. The local external feedback control is generally able to successfully bring and maintain the solution to a suitable response of the reference system, even if it shows to produce also improper bounded solutions especially in the neighborhood of the resonance frequencies, where the overall stability is significantly lowered. Moreover, in such regions the investigation of the evolution of the basins of attraction through the DI tools points out a generalized reduction of the basins' robustness, which leads to critical changes in the safety of the system under slight parameter variations, thus confirming the need of keeping the resonance regions under strict control during practical applications. Differently, the global control technique, expressly aimed at exploiting global features of the system response, proves to succeed in preserving the DI by delaying the erosion of safe basin, thus improving the system safety against jump-to-contact. Clearly, most difficult task in applying this control procedure is related to the actual detection of the bifurcation responsible for the safety loss, which requires the identification of the system saddles together with the relevant manifolds. This passage of the method is undoubtedly computationally burdensome, particularly when the system dynamics displays an involved topological behavior marked by strongly coiled manifolds.

5 Global analysis for practical stability and safe engineering design

5.1 Dynamical integrity as a criterion for practical stability

As observed in the pioneering studies of Thompson [22], theoretical existence and Lyapunov (i.e, classical) stability of a certain solution do not guarantee its actual observability under realistic conditions, i.e., do not entail its *practical* stability. This is because the disturbances always existing in experiments and practice entail uncertainties in the operating initial conditions. Thus, if the system is not sufficiently robust to tolerate them, the actual response may be also completely different from the one theoretically predicted. The basin stability measures and probability density estimations provided by sample based analyses of a given system already give insight on the susceptibility of its response to possible perturbations, thus allowing to explain difficulties possibly encountered in observing theoretical solutions in experimental investigations [85]. However, only the

analysis of dynamical integrity can help catching the rationale behind possibly meaningful discrepancies occurring between theoretical predictions and experimental observations. To this aim, DI charts provide a comprehensive description and understanding of the actual behaviour of a mechanical system in view of its safe practical operation. In the sequel, the matter is illustrated with reference to two specific systems of interest in macro- and micro-mechanics, respectively.

Their mechanical and dynamical features highlight two different, and somehow complementary, situations. Indeed, in the macro-system, attention is paid to the robustness of a special class of solutions (rotations of a pendulum), possibly interesting from a technological viewpoint, which occur outside the potential well bounded by the homoclinic orbits of the periodic hilltop saddle and are not very robust against erosion from competing in-well attractors (pendulum oscillations). Instead, in the micro-device, attention is paid to the overall escape from the potential well surrounded by a homoclinic orbit, irrespective of the in-well solution from which it originates, which leads to a generally unwanted (as, e.g., in MEMS sensor) dynamic pull-in. In both cases, the limits of existence of the theoretical solution are not attained in practice. The practical limits, on the other hand, are associated with acceptable levels of integrity measure, different from case to case but fixed for a specific mechanical system, thus providing evidence of the general interpretative/predictive role played by dynamical integrity.

A macro-mechanical system. The first system is a pendulum parametrically excited by the harmonic vertical motion of its pivot point, which entails pendulum oscillations and/or rotations [37]. It is an archetypal system of interest in nonlinear dynamics, as well as a simple, yet reliable, model to deal with a novel problem of interest in macro-mechanics, i.e., the possible conversion of the oscillatory motion occurring for low/medium values of excitation amplitude into rotary motions of interest in technological contexts like the production of green energy from sea wave motions [32,92].

Constructing several bifurcation diagrams for increasing excitation amplitude at different frequency values, the theoretical range of existence of period-1 rotations in the excitation parameter plane is obtained (Fig. 21). It is bounded on the bottom side by the saddle-node (SN) bifurcation locus where rotating solutions, coexisting with periodic oscillatory motions, originate when increasing the amplitude, and on the top side by the period doubling (PD) bifurcation locus after which a PD cascade leads to chaotic motions then swiftly disappearing via boundary crisis (BC) [33,93]. The experimental investigations, performed on a physical pendulum in a wave flume, were aimed at detecting the lowest and highest amplitudes of excitation at which robust rotations can be realized [92]. Figure 21a shows that experimental rotations exist is a strip of finite magnitude embedded in the central part of the region of theoretical existence, which shrinks for low frequencies. In particular, experimental rotations are not found for large excitation amplitudes, which is somehow expected due to a possibly lower accuracy of the corresponding investigation, and also for low excitation amplitudes, where realizing them should actually be easier. The difference between experimental and theoretical regions of existence of rotations is too large to ensue only from experimental uncertainties. It can be justified by means of a DI analysis, which shows to be of special interest for the rotating solutions that are more susceptible to perturbations than the coexisting oscillatory motions [93].

The key tool for understanding why period-1 rotary solutions are practically observed only in a subset of the stability domain are the integrity profiles of the corresponding basin of attraction, here assumed as safe basin of interest, obtained with uncreasing amplitude at different frequencies. By way of example, the normalized profile of the integrity factor (IF) at ω =1.3 is reported in Fig. 21b, other integrity measures (GIM, LIM) providing profiles with quite similar qualitative patterns [93]. Just after being born via a SN bifurcation at $p_{SN} \approx 0.0476$, the basin of attraction enlarges and its integrity suddenly increases. The subsequent indented region is due to the sudden appearance of various secondary rotations (of periods 6 and 5) via SN bifurcations inside the basin of attraction of the main rotation, thus entailing an instantaneous decrease of the compact part of its safe basin and a fall down of its integrity profile. When those secondary solutions (swiftly) disappear, the whole former safe basin is recaptured by the main rotation, which partially regains its integrity, up to the onset of a period-3 rotation whose basin is more robust than those of the previous secondary solutions and

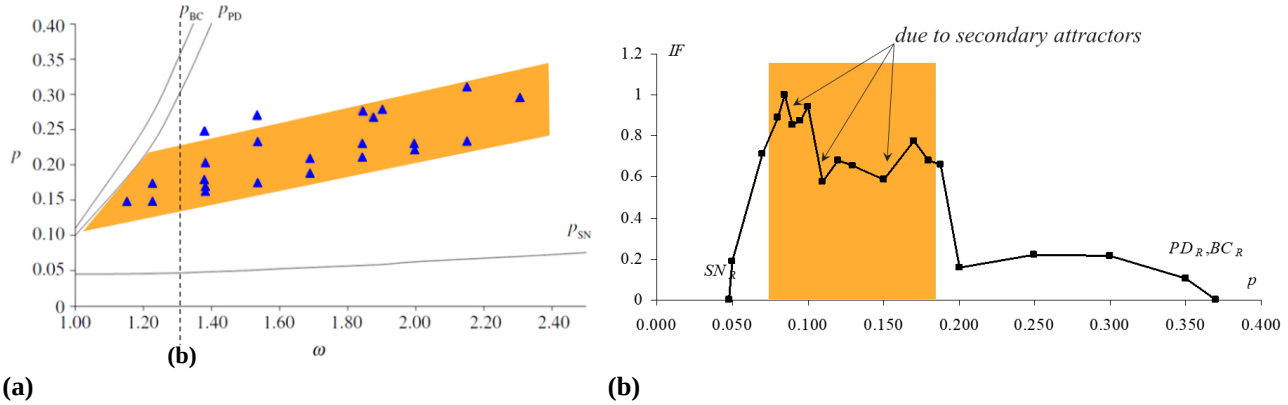

(a) **(b)**

Fig. 21 Parametrically excited pendulum. **(a)** Theoretical (in between SN and PD-BC bifurcation loci) versus experimental (orange strip, with blue triangles) regions of rotations. **(b)** IF profile of period-1 rotation, with the central orange region of relatively high integrity (and a substantially uneroded basin) approximately corresponding to the range of experimentally observed rotations (from [93]). (Colour figure online)

entails the definitive fall down of the profile. To the aim of interpreting Fig. 21a, the main feature of Fig. 21b is that the integrity of the period-1 rotation is high only in about the central part of the whole profile, where the attractor is relatively robust and its basin is nearly uneroded, a phenomenon which qualitatively repeats for different excitation frequencies [93]. Notwithstanding quantitative differences due to a number of experimental uncertainties (mostly concerned with damping), this overall feature explains why the experimental rotations are observed nearly only in the central strip of their wide region of theoretical existence. Note that the low DI results on the profile right and left sides are consistent with the unobserved rotations at both large and low excitation amplitudes, the latter outcome being not so intuitive.

A micro-mechanical device. The second system is a micro-device (an electrically actuated capacitive accelerometer) susceptible to undergo dynamic pull-in when varying the excitation amplitude or frequency. Again, the comparison between outcomes of numerical simulations based on the local stability theory of a single-dof model and experimental data acquired via a frequency-sweeping process highlights a range of practical existence of each attractor that is only a subset of its theoretical stability domain, and a theoretical threshold of inevitable escape that does not reproduce the experimental pull-in bands. As in the pendulum case, the difference between experimental and theoretical regions of escape is too large to be abscribed only to experimental uncertainties, although being certainly related with the effects of disturbances. Owed to its capability to account for such effects, the DI analysis succeeds in providing a theoretical justification of experimental evidences. Details about the experimental exploration of the capacitive accelerometer and the corresponding DI analysis can be found in [57] and [93-95], respectively.

The response chart in the excitation (frequency-electrodynamic voltage) plane of Fig. 22a summarizes the overall scenario of structural safety of the device, as provided by (i) theoretical stability analysis, (ii) experimental investigation, and (iii) DI analysis. Theoretical analysis furnishes the local saddle-node (SN) bifurcation loci delimiting the regions of existence or coexistence of bounded, non-resonant and resonant, periodic solutions. The non-resonant locus (on the left) and the boundary crisis (BC) locus (on the right) entailing disappearance of the in-well chaotic attractor originated from the resonant solution via a sequence of period doublings, represent the overall excitation threshold (in blue colour) above which inevitable escape, i.e. dynamic pull-in, occurs. In turn, the analysis of the physical device provides pull-in data (empty circles in Fig. 22a) whose qualitative envelope via the red curves represents the experimental excitation threshold above

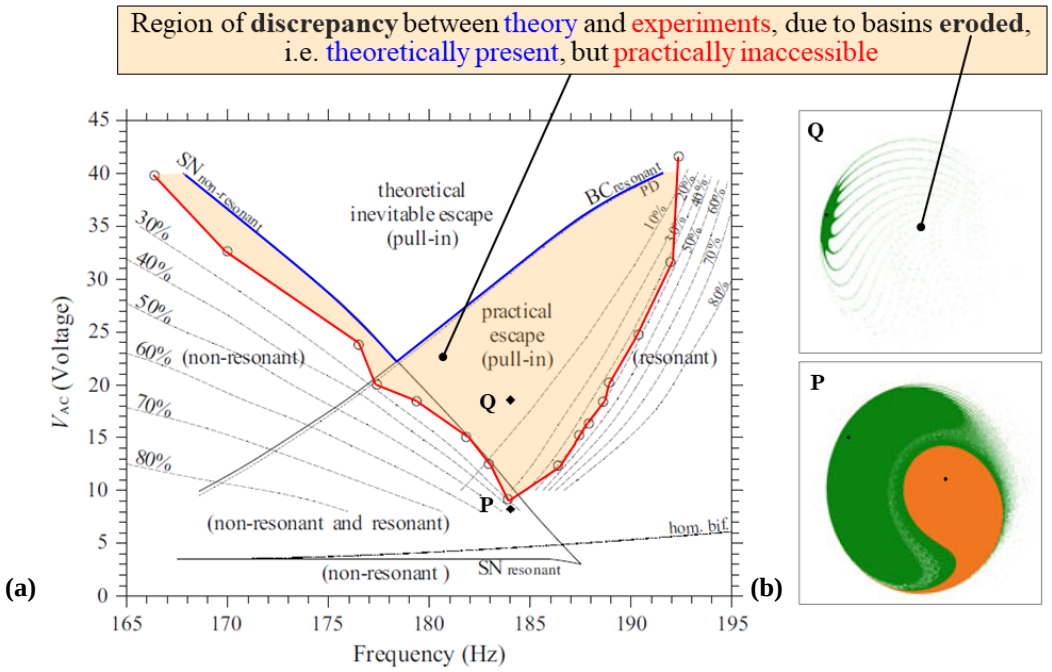

Fig. 22 Electrically actuated capacitive accelerometer. **(a)** Response chart with theoretical (blue) and experimental (red) escape thresholds, and integrity contour lines (dashed). Practical escape region significantly wider than experimental one. Thresholds of practical disappearance of nonresonant/resonant attractors nearly coinciding with iso-integrity lines. **(b)** Initially and fully eroded basin of resonant attractor at points P and Q (from [95]). (Colour figure online)

which pull-in occurs. Comparison of the blue and red loci highlights a general overestimation of the theoretical escape threshold with respect to the experimental one, which is strongly marked in the right part of the chart where the bounded resonant solution should theoretically occur for medium values of the electrodynamic voltage V_{AC}, but is not observed in practice. This is due to the circumstance that, in that area, the resonant basin of attraction, while existing theoretically, is so strongly eroded to become practically inaccessible. This is properly unveiled by the DI analysis, performed by constructing profiles of the local integrity measure (LIM), used for its capability to catch the attractor disappearance, with varying frequency, at different V_{AC} values. The ensuing curves of constant LIM percentage (dashed lines in Fig. 22a), decreasing with increasing V_{AC}, are nearly uniformly distributed on the left side, where they almost reach, with vanishing value, the theoretical (SN non-resonant) threshold of local stability. Instead, on the right side, they are packed within a much lower zone of the chart, quite away from the theoretical (BC resonant) threshold. Thus, by way of example, at point Q (V_{AC} =18.4 V, Ω = 184 Hz) in Fig. 22a, where the (orange) nonresonant basin does not exist any more, the (green) resonant one is also vanishing due to its extremely low integrity (top panel in Fig. 22b): compare with its still relatively integer counterpart at point P (V_{AC} =8.0 V, Ω = 184 Hz, bottom panel in Fig. 22b), where the incursion of the escape (white) fractal tongues close to the boundary of separation from the coexisting non-resonant basin has just started, although both basins are already reduced with respect to the whole well occupied by either one of them at low and high excitation frequencies.

Two aspects are of major interest here: (i) The remarkable coincidence, on both sides, between the thresholds of experimental pull-in (the red loci) and fairly precise LIM contour levels. (ii) The occurrence of the right experimental pull-in for a LIM value still relatively high (30-40%), with the integrity profiles decreasing so steeply at a given frequency, for higher V_{AC} values, to entail a strong susceptibility of the bounded attractor to disturbances (i.e, a low attractor robustness), and the ensuing impossibility to find it in practice. For the considered experimental conditions, the sudden fall of the integrity profile leading to practical pull-in seriously reduces the range of existence of the attractor with respect to the theoretically predicted BC threshold.

Overall, for given values of a control parameter, the possible strong packing of integrity contour lines, which corresponds to a steep decrease of the underlying profile with the other varying parameter and takes place in variable ranges of anyway low values of residual integrity, also corresponds, within a reasonable approximation, to the threshold beyond which practical escape occurs. Thus, for a given attractor, a relatively narrow range of residual integrity levels dividing the whole region of theoretical existence in two different zones, i.e. an area of practical existence and an area of practical disappearance, can be identified. In the former, the attractor can be observed in practice; in the latter, it exists in the theoretical predictions but cannot be practically realized for being highly vulnerable. In this last region, the device cannot be operated in safe conditions with a desired final outcome.

In general terms, the iso-integrity curves allow to properly detect the range where a certain attractor vanishes in practice, and DI charts are valuable theoretical tools for *interpreting* the experimental behaviour. Moreover, they show other contour levels of constant DI percentage, useful for analyzing the effects of different disturbances, e.g. whether the range in which each attractor practically exists may be enlarged (reduced) by decreasing (increasing) disturbances. Thus, the chart goes beyond a specifically investigated case-problem and sheds light onto the general response scenario. Accordingly, it may be used also to *predict* the expected boundaries of disappearance of each attractor. Other micro/nano-mechanical devices, whose experimental outcomes have been interpreted/predicted by DI analyses, are dealt with in [95].

Summarizing, dynamical integrity turns out to be a valuable indicator of the effects of uncertainties in the operating initial conditions and/or in the system model. Relevant charts may serve as guidelines for the engineering design, since, depending on the magnitude of the expected disturbances, they can be used to establish safety factors aimed at operating the system in safe conditions with the desired behaviour. The matter will be addressed in more detail in Sect. 5.3.

5.2 Global dynamics for engineering design

Based on the results summarized and discussed in the previous sections, it is clear that global dynamics plays a fundamental role: (i) in the theoretical/numerical analysis and control of systems and structures, (ii) in the interpretation of relevant experimental results, and also (iii) in the possible prediction of the practical stability (i.e., robust physical observability) of nonlinear dynamic responses of technical interest. In particular, the discrepancy between theoretical and practical stability limits often occurring due to the unavoidable presence of real-world disturbances does not allow to fully exploit the stability range of engineering systems.

Yet, global dynamic effects in terms of response robustness, susceptibility to disturbances, and risk of failure may be taken into proper account in the design stage, pending a number of open issues. These include, among others: (i) The conceptual and, mostly, operational difficulties encountered when moving from the relatively simple low-dimensional models considered until now to the higher-dimensional ones needed to describe the nonlinear dynamics of real structures. (ii) The actual capability of global dynamics approaches to the evaluation of robustness and safety, conducted in a deterministic environment, of indirectly accounting also for the effects of the stochasticity always characterizing real phenomena.

Basin stability approach. The sample-based analysis of the BS approach (see Sect. 3.4) employing Bernouilli trials moves from the difficulties of multidimensional applications and quantifies stability in terms of probability to reach given attractors from random initial conditions. Giving information on coexisting solutions and volumes of their basins of attraction, the sample-based approach provides measures of the corresponding stability. Moreover, in the extended version considering also parameters perturbations, it furnishes the probability of each solution in a given parameter range, along with the most probable solution (the one with dominant basin volume) in distinct sub-ranges: see, e.g., the 2D probability density estimations for six solutions, complementary to each other, of a two-dof system in Fig. 16 of [87]. The overall range of parameter values can thus be subdivided into regions in which there are solutions with high stability measure (i.e., with a clearly dominant basin of attraction), also possibly depending on the occurrence of some resonance, and

regions where an anyway dominant basin coexists with those of other (and possibly many) stable solutions. Susceptibility to parameters perturbations is quite low in the former, and much higher in the latter. Thus, if being interested in solutions that correspond to proper working regimes or have a significantly large range of stability, the effects of changing some parameters to optimize working conditions can be analyzed, and ranges of parameter values that ensure predictable behaviour and reliable operation, of considerable interest from the engineering design viewpoint, can be detected. In summary, the BS method is well suited to get a general and comprehensive overview of *all* practically accessible dynamical states with a relatively low computational effort, certainly much lower than the one which would be necessary with the DI approach, mostly in the case of multi-dof systems.

Yet, differences between the two approaches are concerned mostly with the characterization of the response in phase space. Indeed, in the BS method, strongly different (maximum vs minimum) probabilities of occurrence of one solution, out of two coexisting ones, certainly correspond to different (wider vs smaller) basins. But they do not seem to necessarily entail a correspondingly different (higher vs lower) compactness, as it might be verified by computing integrity factors (IF) even in cross-sections of multidimensional basins: see, e.g., panels (c,d) vs panel (a) in Fig. 18 of [87] for a two-dof mechanical system.

One further, though minor, difference between DI and BS approaches stands in the kind of considered coexisting solutions. Indeed, the former has been initially implemented mostly looking at the safety of a set of bounded solutions (or of a single attractor) against dangerous escape, although the competition between bounded operational solutions can certainly be considered, too. In contrast, the BS concept and operational tools have been implemented mostly looking at the coexistence/competition of bounded solutions, although extensions of the method to systems susceptible to escape (as an often risky failure) can easily be envisaged.

Still based on the BS method, the potential of time-dependent stability measurements along a stable periodic orbit [88] for engineering design has to be further explored. By quantifying time-variable stability margins, the parts of a trajectory where the system is susceptible to perturbations can be identified, and the probability of reaching an adjacent basin boundary can be assessed. Minimum and maximum distances between the attractor and its basin boundary indicate the easiest moment and the least likely one to induce the switch to another attractor, respectively, this kind of information being of interest for possible control purposes in a local (i.e., orbit-oriented) perspective, also in situations where transient escape from a desired basin of attraction may occur. Moreover, calculating the average distance along the trajectory between the attractor and the boundary of its basin can help comparing the stability of coexisting attractors and getting meaningful knowledge about the corresponding probability to reach points on the boundary. Overall, using the underlying sample based approach when the system phase space dimensions increase does not seem to become much more complex, thus making the time-dependent stability evaluations potentially useful for the design of multistable systems.

Summarizing, sample based methods of dynamic analysis allow:

(i) to detect all possible solutions (including hidden and rare attractors) with basin stability greater than some threshold;

(ii) to investigate ranges of stability in multiple parameters space, and the effect of uncertainties in the perturbations (parameters mismatch), with results which enable to assess the robustness of solutions with respect to changes of parameters and to estimate the risk of unwanted behaviours.

One more interesting feature of the BS approach stands in the presentation scheme used for the computational results. Giving up to comprehensively describing the structure of the solutions in geometrical terms – which is nearly impossible for multi-dof models –, it focuses on probability plots providing some main features of the system response in parameters space, and also somehow in phase space, although to a definitely minor extent. Overall, additional knowledge is obtained over more traditional continuation methods, with a computationally affordable effort.

Dynamical integrity approach. With respect to the BS approach providing information on *all* practically accessible dynamical states, DI allows in-depth investigations (still with a relatively low computational effort)

of the actual robustness and safety mostly of *given* dynamical solutions of interest, ranging from a set of in-well and/or bounded solutions (dictating the associated safe basin) up to specific attractors (with their basins) in a given parameter range. In the sequel, the analysis of a case study in which a system's quite rich dynamics is addressed from different perspectives by complementarily using alternative definitions of safe basin and correspondingly different DI measures, allows to shed light on the advanced level of knowledge obtainable about structural safety.

Reference is made to a single-mode model of slacked carbon nanotube electrically actuated, with single potential well and escape direction, focusing on bounded (i.e, in-well) or specific attractors, and their combined or isolated vulnerability to dynamic pull-in [28]. Figure 23 shows three integrity charts in the excitation parameter plane, with the relevant contour lines, for the potential well (a), for the probability of occurrence of two main attractors (b), and for their practical disappearance (c), as obtained with the correspondingly 'best' suited IF, GIM, and LIM indicators, respectively. Figure 23a shows a (red) range of medium/low values of voltage, where the variably high IF values highlight that safe conditions, corresponding to all trajectories originated in the safe basin (i.e. the potential well) ending up to a bounded motion (i.e., whatever attractor in the potential well), can be robustly realized. This range is worth of further analysis aimed at detecting the attractor which may be expected to effectively operate the device, whereas the upper ranges (with packed contour lines of strongly decreasing integrity, and further very low IF) are more and more vulnerable to pull-in and must be avoided in design. Focusing on the medium/low voltage range, the GIM charts in Fig. 23b indicate that only two main attractors, out of the many coexisting in the potential well, can be actually realized with acceptable robustness, although it meaningfully changes from one sub-range to another, with the anyway marked danger of non-occurrence at higher voltage values already alerted by the IF analysis of the potential well. However, due to small compact parts of their basins in various parameter ranges, both attractors are susceptible to practically disappear, i.e. trajectories originated in the correspondingly safe basins may jump to

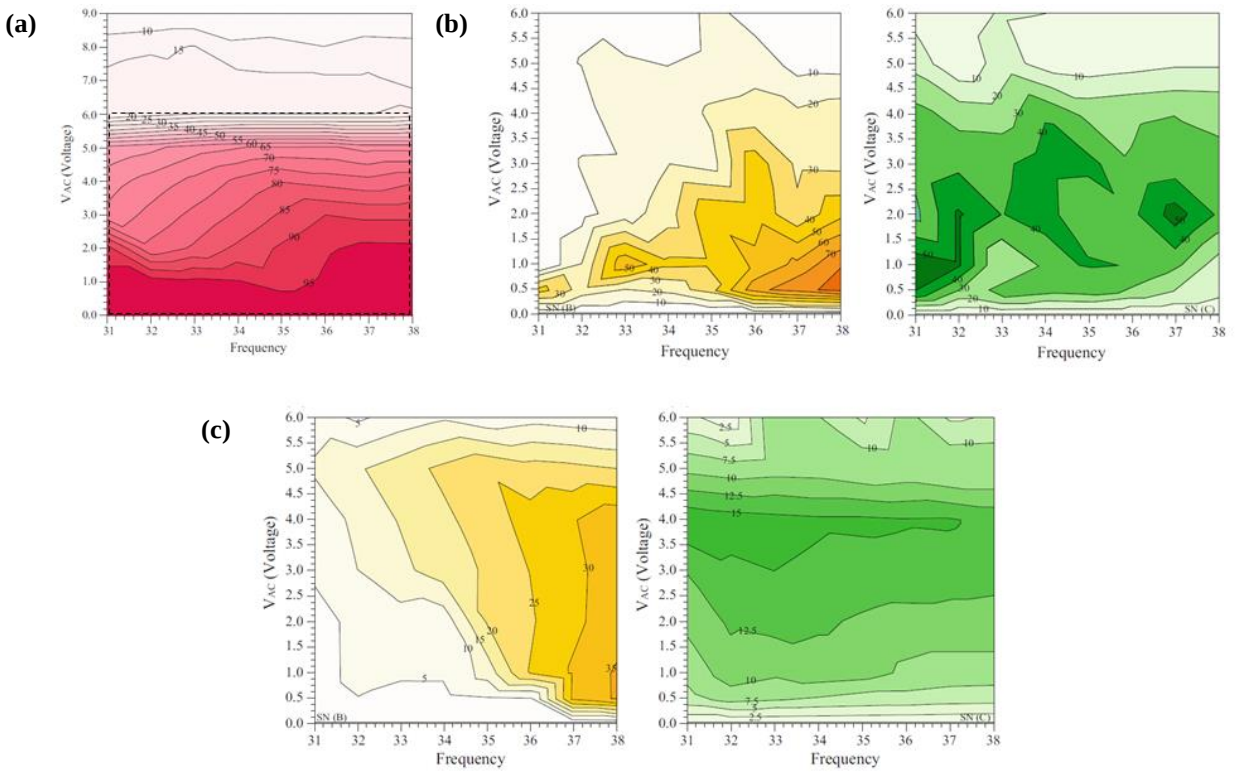

Fig. 23 Electrically actuated carbon nanotube. **(a)** IF chart for the potential well with safe (red) area, in large region of parameters space. **(b)** GIM and **(c)** LIM charts for two main competing in-well attractors, in the zoomed region of parameters space where they exist with variable probability (GIM) but quite low practical robustness (LIM) (from [24]). (Colour figure online)

one of the highly probable coexisting motions, either bounded or, most likely, unbounded (i.e., pull-in). This is highlighted by the quite low LIM values in the charts of Fig. 23c, which highlight how the high probability to realize those attractors, evidenced by the GIM analysis not accounting for basins' compactness, does not guarantee to keep the device actually operating with them, due to the effects of unavoidable disturbances taken into account by the LIM.

Overall, despite the richness of system's behaviour, the combined use of the IF and the GIM restricts it down to a small range of actual parameters and to a few operating attractors, and the LIM highlights the actual possibility to operate the device with a desired attractor, due to the topological sensitivity of its basin to inevitable uncertainties. Thus, a synergic combination of information obtained by DI analyses making use of different safe basins and well-suited indicators of the corresponding robustness turns out to be of great importance for a reliable engineering design.

Of course, pursuing investigations of this kind and getting a similar knowledge in the case of higher-dimensional models is much more complicated, in terms of calculation of multidimensional basins of attraction needed for integrity analyses and associated aspects of geometrical representation/visualization. Safe basins are generally computed by one of several variants of the classical cell mapping method [5]. For systems with many dof, upon earlier implementations of cell mapping in parallel computers [96,97], remarkable improvements in the development of parallelized computational algorithms have been made in the last few years [98-102], with approaches that permit to analyze in a reasonable computational time a large set of initial conditions with a resolution sufficient to properly determine basins of attraction. To implement efficiently the cell mapping method on massive parallel architectures, the algorithmic processes have to be balanced properly between memory operations and numerical integrations [102]. In the DI perspective, one important issue is concerned with the computational efficiency of a parametric analysis of how safe basins vary with a governing control parameter. In this respect, use of parallel computation with reasonable CPU time allows to consider nearly continuous variations of a control parameter, thus succeeding to highlight fine aspects of integrity/erosion profiles [29], and to overall improve results based on finite (and commonly large) variations of the parameter, due to computational constraints.

It is however worth noting that, even without resorting to parallel computing, a meaningful step forward in the evaluation of DI of multidimensional systems has been made via the development of numerical methodologies based on the Monte Carlo approach for the estimation of integrity measures by means of sampling initial conditions [46]. In such context, the GIM is defined as a multiple integral, and is obtained though a classical application of the Monte Carlo approach, by verifying the proportion of initial conditions that either belong or do not belong to a given basin. In turn, the LIM and IF are modelled as optimization problems, and are evaluated within stochastic processes by taking the minimum distance between the attractor and sampled initial conditions of competing basins, and the maximum distance out of the minimum ones between all sampled initial conditions, respectively. The convergence of sample averages to the real values is guaranteed by the hypothesis of ergodicity and by checking the evolution of sample variances. In some sense, the proposed procedure embeds the computational advantages of sample based approach in phase space into the safety assessment capability of the DI and, like the BS approach, it does not require direct construction of basins of attraction nor use of computationally expensive procedures. Application to a discrete model of truss, with a dynamics developing in up to a six-dimensional phase space, has shown quite reliable results, obtained with smaller amounts of processing cycles than those necessary in classical DI evaluations based on brute force method or simple cell mapping (where applicable), and an advantage increasing with an increase in the phase space dimension.

Another problem in the DI analysis of multi-dof systems consists of the nearly unsolvable difficulties to achieve an effective visualization of multidimensional basins of attractions and also, to a certain extent, of the integrity outcomes ensuing from systematic, and certainly heavy, calculations of solutions' (basins') robustness in phase space (parameter space). Indeed, along with computational aspects, topological/geometrical ones are the other characterizing ingredient of the DI approach to global safety of

systems, that distinguishes and, for multi-dof systems, penalizes it with respect to purely computationally-driven approaches, which keenly give up assessing the topological structure of the phase space. No doubts that, for multi-dof systems, only partial (2D or, at maximum, 3D (see [29])) representations of actual multidimensional basins can be obtained by means of properly chosen hyper cross-sections, typically the 2D ones used in Sect. 2 for the thermochanical plate and in other studies on systems' global dynamics [46,47,49-51,103-106]. However, the amount of information and useful understanding on system dynamics, obtainable from suitably selected cross-sections also in the DI perspective, e.g. [64,79 (Fig. 23)] and some of the above works, suggests to not give up catching at least some topological aspects of multidimensional basins of attraction, while of course being far away from getting their overall structure. As regards visualization of systems' stability/integrity, attempts have been made recently to characterize safe working regions based on 3D integrity manifolds combining the representation of an integrity measure in terms of a design parameter with its actual localization in phase-space [29].

Needless to say that the application to multi-dof systems of the global bifurcation control discussed in previous sections and successfully used to delay the loss of DI in a great variety of single-dof models, appears nearly impractical at the current stage of knowledge. This is concerned with both topological and computational aspects. Indeed, it requires preliminary detection of the saddle manifolds whose intersection actually triggers the erosion phenomena, which is an involved item to be conducted numerically already for single-dof models, except when hilltop saddle manifolds are the responsible ones. Apart from the overall complexity of the global bifurcation events underlying fractality, whose theoretical paradigms should likely be revisited for multidimensional systems, the design and implementation of a similar globally-oriented technique for possible optimal control of their DI is a definitely challenging issue in both theoretical and computational terms.

All of the above difficulties highlight how the formulation of effective low-order ROMs of a given structure, able to exhibit the main relevant phenomena of nonlinear modal interaction and energy transfer occurring over large frequency bands, keeps all of its importance also, if not even mostly, in the global understanding and safety perspective. Reliable low-order models may be used both in a preliminary design stage and as tools complementary to richer computational models/methods (like finite elements) for getting otherwise unobtainable, and thus unexploitable, information on the structure's global dynamics.

Effects of stochasticity. The role played in the analysis, control and design of nonlinear systems by unavoidable practical uncertainties in system's and excitation's features is fundamental. From the viewpoint of computational methods for global analysis and control design, a recent survey on cell mapping techniques also accounting for the performances obtainable through the use of massively parallel computing technologies has been concerned with stochastic and fuzzy dynamical systems, too [100]. As regards the BS method, it has been already discussed how intensive sample-based analyses allow to quantify the probability of reaching a given attractor from random initial conditions and parameter values, both accounting for existing perturbations/uncertainties. Problems possibly arising in the basin stability estimation for stochastic systems have been also addressed in the literature, focusing on the algorithmic errors ensuing from intricate phase space geometries, with extended fractal basin boundaries and riddled or intermingled basins of attraction [107].

As regards erosion/integrity phenomena, the effects of a noise excitation superimposed to a deterministic one and/or of randomness of system parameters have been investigated in some papers, considering archetypal oscillators and ROMs of slender structures liable to unstable buckling. Indeed, due to the imperfections and disturbances always present in real situations, instability of these structures in a dynamical environment usually occurs at load levels much lower than the static buckling load of perfect structures. The influence of random noise and system parameter uncertainties on the dynamic instability of structural systems liable to buckling was discussed for an archetypal oscillator with asymmetric post-buckling behaviour [38,40], and for the axially excited cylindrical shell [51,53], other references on the effects of stochasticity being also reported in [77].

Overall, stochasticity may meaningfully affect a system's structural safety, with modifications of the topological pattern of the erosion and a general aggravation of the process up to a generally earlier escape.

However, results in the excitation parameter space are quite scattered with the forcing frequency, and meaningfully depend on the standard deviation of the random noise excitation superposed to the deterministic one or on the perturbed value of the system parameter assumed as a random variable with given probability density function. A very small influence is found on the basin of attraction and the related integrity measures for low levels of the harmonic load, whereas for load levels closer to escape the influence of random noise on basin erosion becomes important, with a nontrivial decrease of integrity.

In the DI-driven safety perspective, two main outcomes (although so far evidenced only for relatively few systems) deserve a special interest.

(i) The comparison between basins of attraction under deterministic or nondeterministic load in the decreasing part of the corresponding integrity profiles highlights that the random noise adds a certain degree of unpredictable outcome from the initial conditions close to the basin boundary, but leaves the residual compact subset of the safe basins substantially unchanged. This can be seen, e.g., in Fig. 24, which shows the two basins of an elastic von Mises truss, which is an archetypal model for bistable structures undergoing dynamic snap-through under transverse excitation [41]. In the white area of the undeterministic basins the response outcome is uncertain, but the compact part of both the competing basins in the right well and the single basin in the left well is affected by the presence of a relatively high added random noise only marginally, with respect to the corresponding deterministic basins. This guarantees normalized IF values (which is a measure accounting for basin compactness) nearly unchanged with respect to the deterministic ones, and still quite high (around 0.9). Similar outcomes have been obtained in cross-sections of a multidimensional ROM of an axially excited cylindrical shell [51].

(ii) Escape results in the excitation parameter space obtained by considering different possible uncertainties turn out to be almost packed around, or just below, the deterministic stability threshold, thus staying above integrity contour levels characterized by quite low values [38]. This is the case for, e.g., an asymmetrically stiffened inverted pendulum subjected to vertical dead load, which is a system liable to unstable buckling. As shown in Fig. 25, its dynamic stability boundaries obtained by considering uncertainties in all system parameters, except the lateral harmonic excitation, lie above the 40% iso-integrity curve of the system with reference parameter values [38,78], when the dynamic excitation is applied either slowly (black dots) or suddenly (red dots). This highlights how the scattered decrease of stability threshold entailed by consideration of uncertainties takes place, as a rule, within a range of very low residual integrity, in

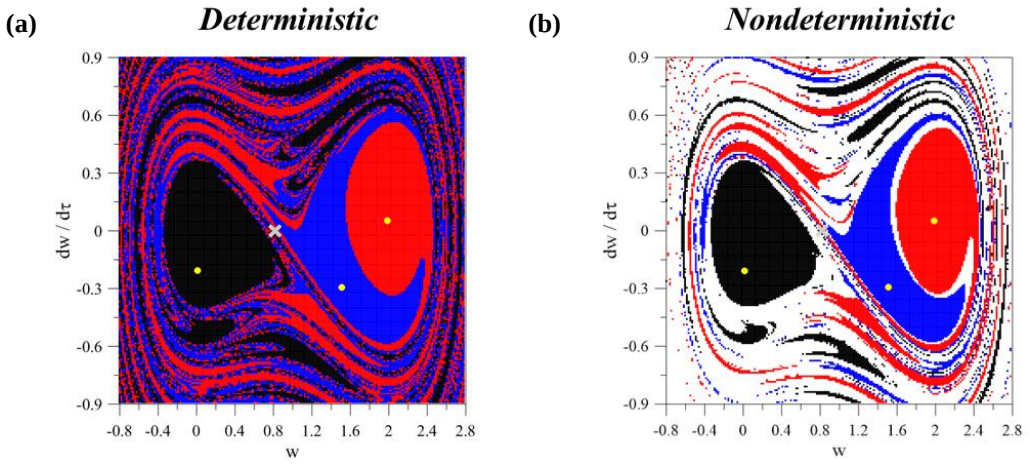

Fig. 24 Elastic von Mises truss model under transverse excitation. Basins of attraction under **(a)** deterministic or **(b)** nondeterministic (with a relatively high added random noise) load, in the decreasing part of the corresponding integrity profiles. (Colour figure online)

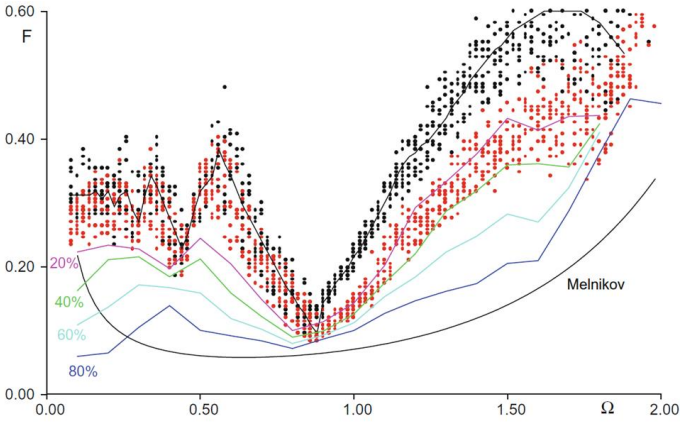

Fig. 25 Asymmetrically stiffened inverted pendulum liable to unstable buckling. Escape thresholds by considering uncertainties in all system parameters and a suddenly (red dots) or slowly (black dots) applied dynamic load, with also integrity contour levels of the system with reference parameter values and the Melnikov lower bound of homoclinic bifurcation [38,78]. (Colour figure online)

between the deterministic escape threshold and some corresponding upper iso-integrity curve, which turns out to be unacceptable from the design viewpoint.

Previous results need confirmation through more extended and systematic investigations aimed at further clarifying the relationship between influence of stochasticity on global dynamics and system dynamical integrity, to be conducted in a variety of situations and for different mechanical systems. In this respect, apart from results recently obtained about specific noise-induced chaotic-attractor escape routes [108], on-going studies showing the effects of forcing uncertainties on the attractors' probability density functions and basins of attraction, are to be mentioned [109]. They are obtained by the generalized cell mapping employed together with a modal stochastic differential equation of Itô type solved by the stochastic Runge-Kutta method, although outcomes in terms of associated dynamical integrity are not yet available.

However, up to the current state of knowledge, it seems possible to conjecture that pursuing the system safety via a criterion of minimum required value of residual integrity, properly measured by considering the sole compact part of the basin, may also account for the decrease of stability threshold entailed by possible uncertainties, although in a solely indirect way. This further highlights the effectiveness and versatility of a DI-driven approach to design.

5.3 Towards a novel paradigm for load carrying capacity and aware design

The DI approach capability to predict discrepancies of practical vs theoretical thresholds for the occurrence of a pursued system dynamics highlights his tremendous potential for increasing the actual usability of systems and structures via a design criterion exploiting the concept of *minimal* allowed residual integrity. In the case of dangerous escape, in which discrepancy consists of even important lowerings of the stability threshold, the DI approach may guarantee the actual system safety and load carrying capacity.

In general terms, as already mentioned, the unavoidable disturbances of the real-world do not allow to fully exploit ranges of theoretical stability. This is one main constraint in the operational life of engineering systems, faced by the technical community, since long time, via the introduction of large safety factors in the design stage. However, an approach to system safety that completely overlooks the dynamics behind the problem may not provide the designer with a capability to overcome practical barriers. In contrast, the DI approach allows to catch the reasons behind the observed discrepancies, and gives hints towards a completely different, knowledge-based, criterion for design, in which attractors' robustness and basins' erosion phenomena are properly taken into account, and the level of perturbations that the system can support in terms of global behaviour are established.

In this respect, robustness/erosion profiles and integrity charts are useful guidelines for aware and safe design not only as regards predicting boundaries of actual disappearance of whatever attractor but also to understand how decreasing (increasing) perturbations entails enlarging (reducing) its range of practical existence. Worth information can thus be obtained as to the variety of response scenarios possibly ensuing from consideration of different disturbances, moving forward from the case-study specifically analyzed.

This is one side of the coin. The other side, to be addressed in parallel, consists of carefully assessing the magnitude of the disturbances that the structure is expected to undergo during its life, based on the maximum allowable tolerances prescribed in fabrication/construction processes, on the procedures implemented for a reliable quality control, and on the uncertainty quantification issues taken into account. In this last respect, it is worth noting that stochastic arguments are solely needed to determine the average amplitude of the *expected* perturbations, to be considered as the *admissible* ones for establishing a value of acceptable residual integrity such to secure the realization of a given operational condition for the system. It could be said that the increased level of knowledge and understanding of system nonlinear behaviour provided by dynamical integrity allows to deal with uncertainties in a substantially deterministic framework.

The improved capability to accurately predict safe parameters, in particular close to resonances and/or bifurcations, may permit to consciously exploit the *actual* system resources in terms of load carrying capacity, which instead in the current design framework turns out to be substantially reduced precisely as a result of the renunciation to understand and govern the underlying nonlinear/global phenomena. The enhanced usability of systems and structures attainable at both macro- and micro/nano-scales by a conscious exploitation of the available knowledge on global behaviour is apparent, with all ensuing benefits in technological terms.

Following [24,77], a schematic (yet very close to real) representation of the advantages obtainable in terms of awarely evaluated load carrying capacity by using a DI-driven design criterion is provided in Fig. 26, which illustrates the two-parameter (excitation amplitude and frequency) safety chart of a generic softening system (susceptible to escape), in the neighborhood of a resonance frequency. The softening backbone curve represents the resonance nonlinear frequency, and the stability/bifurcation threshold resulting from an envelope of local bifurcation points is the upper boundary of the region of theoretical stability, beyond which inevitable escape (pink area) occurs. In a neighborhood of the resonance frequency, the incursive vertex denotes a marked fall down of the stability region, to be taken properly into account in the design. Overall, increasing the excitation amplitude, the stability region becomes more varied and complex especially around the resonance, where the practical region may be reduced even more than the theoretical one. In this context, the conventional approach adopted within the technical community to guarantee safe conditions consists of relying only on the part of the parameter space where the nonlinear phenomena entailing dramatically dangerous effects are not experienced. The system is thus designed to operate only in the linear (or very close to linear) regime, which is the sole one to be considered fully reliable. In the design stage, this is achieved by introducing large safety factors such to establish an adequate distance of the operating area away from the zone of nonlinear behaviour. In Fig. 26, the ensuing safe threshold to be not overcome delimits the lowest (dark green) region. Generally, the threshold is assumed even independent of varying parameters, e.g., it is not raised up when the system is operated away from resonance, as it would be theoretically (and also practically) allowed if somehow accounting for its nonlinear behaviour.

Overall, the conventional approach intentionally overlooks the whole system dynamics and guarantees safe operating conditions only in a narrow range of quite low excitation amplitudes, thus beeing very conservative. Indeed, as also proven by experiments in different fields (see Sect. 5.1 and [95]), the system can be reliably operated in practice also in a wider region of parameters space (although smaller than the one of theoretical stability), provided the nonlinear and complex, yet non-necessarily dangerous, dynamics of the system is properly taken into account. If this is overlooked, a large part of the system capacity potential is lost, in constrast with the growing need to take advantage of the variety of nonlinear features for designing and fabricating systems with higher performances and safety characteristics, mostly in advanced technological contexts (see, e.g., [110,111]). Earlier accounts of the nonlinear and also global behaviour of dynamical

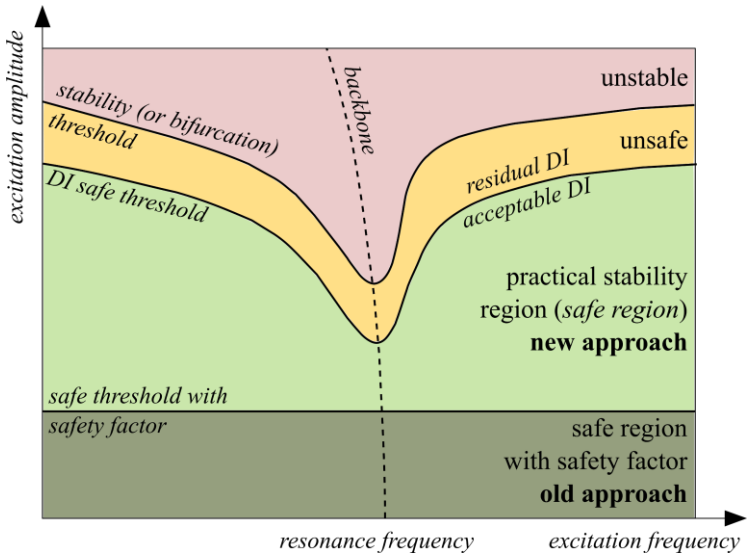

Fig. 26 Schematic safety chart for a generic softening system subjected to harmonic excitation. The light green-yellow-pink sequence of colours for increasing excitation amplitude corresponds to the DI strip one in Fig. 10. (Colour figure online)

systems (based on the Melnikov criterion for homo/heteroclinic bifurcation of the hilltop saddle, or other criteria, see [112]) already suggested possible widenings of their operational range. However, only a full exploitation of global safety concepts can pave the way to a novel approach, capable to identify reliable thresholds for safe engineering design such to take advantage of the system actual capacity potential.
In Fig. 26, an admissible residual dynamical integrity (DI safe threshold) is established, corresponding to a level of perturbations which represent the magnitude of expected disturbances. The regionof parameters space below the selected iso-integrity curve is safely allowed in the design. It meaningfully broadens (dark plus light green area) the safe region of the conventional approach, while consciously accounting also for some main features of global nonlinear behaviour, i.e., the fall down of both the escape threshold and the integrity contour lines occurring at nonlinear resonance. Above the enlarged safe area, the solution theoretically exists up to its stability boundary (yellow area), but it is practically unsafe from the global dynamics viewpoint because of the highly dangerous effects of too large disturbances. Of course, further above, the escape becomes inevitable (pink area). Figure 26 is a schematic, but qualitatively similar charts for more concrete case studies have been presented in [79,95].

The considered example clearly shows the DI approach to design. When varying a main control parameter (e.g., increasing the excitation amplitude), the designer is called to fix the minimum acceptable value of dynamical integrity, i.e., the maximum allowed change of initial conditions which can be safely supported by the system with respect to the desired operating solution. In traditional terms, this corresponds to fixing a kind of safety factor with respect to the unwanted event, under given values of the other control parameters; but the context is now totally different from the conventional approach, because of being based on the clear identification, comprehensive knowledge, and controllability of the factors governing the system behaviour. This allows to increase the operating range of the system and to exploit the whole safe region in parameters space, in an aware but not too conservative way.

In summary, dynamical integrity succeeds in offering a deep insight of system's expected behaviour, and allows establishing a *novel paradigm* for safe and aware engineering design which, to a certain extent, also indirectly accounts for undeterministic aspects. All of this may meaningfully affect the awareness of practitioners of mechanics about the *importance* of global analysis for an improved and modern use of systems and structures in engineering. In a longer term perspective, this can also pave the way to the introduction of technical recommendations fully accounting for, and also possibly exploiting, the nonlinear and global

behaviour of systems within a new generation of standards and codes. Widening the range of reliable and safe operation of dynamical systems, and revisiting the conception/development of structures and devices based on novel and aware design criteria, may entail meaningful technological enhancements as regards both the increase of performances and the cost reduction of engineering systems.

6 Conclusions

The fundamental role played by global dynamics in the analysis, control and design of mechanical systems and structures has been discussed, focusing on the geometrical and computational aspects which underly the assessment of robustness and safety of the relevant response.

As regards the analysis, among various situations to be possibly considered, the meaningful contribution of global dynamics to an overall understanding of the response scenario in a continuous system has been addressed by referring to a coupled thermomechanical plate in which the field variables of the two participating physics evolve on non-trivially different time scales. This entails important effects of the slow transient dynamics of the thermal field on the notably faster steady dynamics of the mechanical field which, while suitably working with a minimal, yet reliable, reduced order model, can be solely unveiled via in-depth numerical investigations of the structure's global dynamics in its actual multidimensional phase space.

Then, attention has been devoted to the global bifurcation events triggering the erosion of basins of attraction under a varying control parameter, with final ending up of the response of a multistable system to a different bounded dynamics or to unbounded escape. The need to comprehensively describe and understand mechanisms and topological features of the erosion phenomenon via in-depth analyses of the system dynamical integrity has been discussed, along with the highly beneficial effects that an optimal control of the global event actually governing the overall response scenario may have on avoiding, or at least delaying, the sudden loss of system robustness which rapidly leads to unwanted or highly dangerous final outcomes. The above aspects have been first addressed in general terms, by revisiting some main underlying conceptual and operational items, and then exemplarily illustrated for a softening reduced model of atomic force microscope, dwelling in detail on the capability of global dynamics to comprehensively analyse and control its robustness and actual safety margin.

Three main items have been dealt with in the last part of the article. First, the possibility to explain discrepancies between theoretical predictions provided by classical, locally-driven, stability analyses and the actual experimental response of physical systems in macro- or micro-mechanics has been addressed, highlighting the important role that dynamical integrity can play as an interpretative and predictive criterion for the practical stability of systems and structures. Then, referring to two distinct (basin stability and dynamical integrity) approaches based on global analysis of systems, a survey of the information obtainable in terms of response robustness, susceptibility to disturbances, and risk of failure has been presented. The peculiarities and the different capability of the two approaches to deal with also higher-dimensional models of real structures and to account for the effects of stochasticity have been discussed. Finally, the challenging perspective opened by the dynamical integrity approach to system robustness as regards revisiting the safety paradigm currently used in the design of engineering systems has been addressed. In particular, a design criterion exploiting the concept of minimal allowed residual integrity, to be established based on a careful assessment of the expected disturbances, and indirectly accounting for the effects of uncertainties, has been discussed. It may fruitfully allow an aware exploitation of the actual load carrying capacity of engineering structures, such to enhance their usability in wider ranges of control parameters and in a variety of technological applications.

Acknowledgments Contributions of Stefano Lenci and Paulo Gonçalves to the research background of this feature article are acknowledged.

Compliance with ethical standards

Conflicts of interest The authors declare that they have no conflict of interest.

References

1. Guckenheimer, J., Holmes, P.: Nonlinear Oscillations, Dynamical Systems, and Bifurcation of Vector Fields. Springer, New York (1983)
2. Wiggins, S.: Introduction to Applied Nonlinear Dynamical Systems and Chaos. Springer, New York (1990)
3. Thompson, J.M.T., Stewart, H.B.: Nonlinear Dynamics and Chaos. Wiley, Chichester (1986)
4. Strogatz, S.H.: Nonlinear Dynamics and Chaos. Addison-Wesley, New York (1994)
5. Hsu, C.S.: Cell to Cell Mapping: A Method of Global Analysis for Nonlinear Systems. Springer, New York (1987)
6. Ott, E., Sauer, T., Yorke, J.A.: Coping with Chaos. Wiley, New York (1994)
7. Rega, G.: Nonlinear dynamics in mechanics and engineering: 40 years of developments and Ali H. Nayfeh's legacy. Nonlinear Dyn. **99**(1), 11-34 (2020)
8. Settimi, V., Saetta, E., Rega, G.: Nonlinear dynamics of a third-order reduced model of thermomechanically coupled plate under different thermal excitations. Meccanica (2020). DOI: 10.1007/s11012-019-01117-w
9. Saetta, E., Rega, G.: Third-order thermomechanically coupled laminated plates: 2D nonlinear modelling, minimal reduction and transient/post-buckled dynamics under different thermal excitations. Compos Struct **174**, 420-441 (2017)
10. Doedel, E., Oldeman, B.: AUTO-07p: Continuation and bifurcation software for ordinary differential equations. Concordia University Press, Montreal (2012)
11. Katz, A., Dowell, E.H.: From single well chaos to cross well chaos: A detailed explanation in terms of manifold intersections. Int. J. Bif. Chaos **4**, 933-941 (1994)
12. Rega, G., Lenci, S., Thompson, J.M.T.: Controlling chaos: The OGY method, its use in mechanics, and an alternative unified framework for control of non-regular dynamics. In: Thiel, M., Kurths, J., Romano, C., Moura, A., Károlyi, G. (eds.) Nonlinear Dynamics and Chaos: Advances and Perspectives, pp. 211-269, Springer (2010)
13. Lenci, S., Rega, G.: Optimal control of homoclinic bifurcation: Theoretical treatment and practical reduction of safe basin erosion in the Helmholtz oscillator. J. Vibration Control **9**, 281-315 (2003)
14. Lenci, S., Rega, G.: Forced harmonic vibration in a system with negative linear stiffness and linear viscous damping. In: Kovacic, I., Brennan, M. (eds.) The Duffing Equation. Non-linear Oscillators and Their Behaviour, pp. 219-276, Wiley (2011)
15. Lenci, S., Rega, G.: A unified control framework of the nonregular dynamics of mechanical oscillators. J. Sound Vibr. **278**, 1051-1080 (2004)
16. Lenci, S., Rega, G.: Heteroclinic bifurcations and optimal control in the nonlinear rocking dynamics of generic and slender rigid blocks, Int. J. Bif. Chaos **15**(6), 1901-1918 (2005)
17. Orlando, D., Gonçalves, P.B., Rega, G., Lenci, S.: Influence of modal coupling on the nonlinear dynamics of Augusti's model. J. Comput. Nonlinear Dyn. **6**(4), 041014 (2011)
18. Gendelman, O.V.: Escape of a harmonically forced particle from an infinite-range potential well: a transient resonance. Nonlinear Dyn. **93**, 79–88 (2018)
19. Gendelman, O.V., Karmi, G.: Basic mechanisms of escape of a harmonically forced classical particle from a potential well. Nonlinear Dynamics **98**(4), 2775–2792 (2019)
20. Zhong, J., Virgin, L.N., Ross, S.D.: A tube dynamics perspective governing stability transitions: an example based on snap-through buckling. Int. J. Mech. Sci. **149**, 413–428 (2018)
21. Zhong, J., Ross, S.D.: Geometry of escape and transition dynamics in the presence of dissipative and gyroscopic forces in two degree of freedom systems. Commun. Nonlinear Sci. Numer. Simulat. **82**, 105033 (2020)
22. Thompson, J.M.T.: Chaotic phenomena triggering the escape from a potential well. Proceedings of the Royal Society of London A **421**, 195–225 (1989)
23. Lenci, S., Rega, G.: Load carrying capacity of systems within a global safety perspective. Part I. Robustness of stable equilibria under imperfections. International Journal of Nonlinear Mechanics **46**, 1232–1239 (2011)
24. Rega, G., Lenci, S., Ruzziconi, L.: Dynamical integrity: A novel paradigm for evaluating load carrying capacity. In: Lenci, S., Rega, G. (eds.) Global Nonlinear Dynamics for Engineering Design and System Safety, CISM Courses and Lectures 588, pp. 27-112, Springer Nature (2018)

25. Thompson, J.M.T.: Dynamical integrity: Three decades of progress from macro to nano mechanics. In: Lenci, S., Rega, G. (eds.) Global Nonlinear Dynamics for Engineering Design and System Safety, CISM Courses and Lectures 588, pp. 1–26, Springer Nature (2018)
26. Soliman, M.S., Thompson, J.M.T.: Integrity measures quantifying the erosion of smooth and fractal basins of attraction. Journal of Sound and Vibration **135**, 453–475 (1989)
27. Lenci, S., Rega, G.: Optimal control of nonregular dynamics in a Duffing oscillator. Nonlinear Dynamics **33**, 71–86 (2003)
28. Ruzziconi, L., Younis, M.I., Lenci, S.: Multistability in an electrically actuated carbon nanotube: a dynamical integrity perspective. Nonlinear Dynamics **74(**3), 533–549 (2013)
29. Belardinelli, P., Lenci, S., Rega, G.: Seamless variation of isometric and anisometric dynamical integrity measures in basins' erosion. Communications in Nonlinear Science and Numerical Simulation **56**, 499–507 (2018)
30. Thompson, J.M.T., Ueda, Y.: Basin boundary metamorphoses in the canonical escape equation. Dynamics and Stability of Systems **4(**3–4), 285–294 (1989)
31. Younis, M.I.: MEMS linear and nonlinear statics and dynamics. Springer, New York (2011)
32. Nandakumar, K., Wiercigroch, M., Chatterjee, A.: Optimum energy extraction from rotational motion in a parametrically excited pendulum. Mechanics Research Communications **43**, 7–14 (2012)
33. Lenci, S., Rega, G.: Experimental versus theoretical robustness of rotating solutions in a parametrically excited pendulum: A dynamical integrity perspective. Physica D: Nonlinear Phenomena **240**, 814–824 (2011)
34. Thompson, J.M.T., Rainey, R.C.T., Soliman, M.S.: Ship stability criteria based on chaotic transients from incursive fractals. Philosophical Transactions of the Royal Society of London A **332(**1624), 149–167 (1990)
35. Thompson, J.M.T.: Designing against capsize in beam seas: Recent advances and new insights. Applied Mechanics Reviews **50**, 307–325 (1997).
36. Rega, G., Lenci, S.: Dynamical integrity and control of nonlinear mechanical oscillators. J. Vibr. Control **14**, 159-179 (2008)
37. Lenci, S., Rega, G.: Competing dynamic solutions in a parametrically excited pendulum: Attractor robustness and basin integrity. Journal of Computational and Nonlinear Dynamics **3**, 041010-1–9 (2008)
38. Gonçalves, P.B., Santee, D.M.: Influence of uncertainties on the dynamic buckling loads of structures liable to asymmetric post-buckling behavior. Mathematical Problems in Engineering, Article ID 490137 (2008)
39. Lenci, S., Rega, G.: Load carrying capacity of systems within a global safety perspective. Part II. Attractor/basin integrity under dynamic excitations. International Journal of Nonlinear Mechanics **46**, 1240–1251 (2011)
40. Silva, F.M.A., Gonçalves, P.B.: The influence of uncertainties and random noise on the dynamic integrity analysis of a system liable to unstable buckling. Nonlinear Dynamics **81**, 707–724 (2015)
41. Orlando, D., Gonçalves, P.B., Rega, G., Lenci, S.: Influence of transient escape and added load noise on the dynamic integrity of multistable systems. Int. J. Non-Linear Mechanics **109**, 140-154 (2019)
42. Lenci, S., Orlando, D., Rega, G., Gonçalves, P.B.: Controlling practical stability and safety of mechanical systems by exploiting chaos properties. Chaos **22**(4), 047502-1–15 (2012)
43. Lenci, S., Orlando, D., Rega, G., Gonçalves, P.B.: Controlling nonlinear dynamics of systems liable to unstable interactive buckling. Procedia IUTAM **5**, 108–123 (2012)
44. Eason, R.P., Dick, A.J., Nagarajaiah, S.: Numerical investigation of coexisting high and low amplitude responses and safe basin erosion for a coupled linear oscillator and nonlinear absorber system. J. Sound Vib. **333**, 3490–3504 (2014)
45. Piccirillo, V., do Prado, T.G., Tusset, A.M., Balthazar, J.M.: Dynamic integrity analysis on a non-ideal oscillator. Mathematics in Engineering, Science and Aerospace **11(**3), 1-7 (2020)
46. Benedetti, K.C.B., Gonçalves, P.B., Silva, F.M.A.: Nonlinear oscillations and bifurcations of a multistable truss and dynamic integrity assessment via a Monte Carlo approach. Meccanica (2020). https://doi.org/10.1007/s11012-020-01202-5
47. De Freitas, M.S.T., Viana, R.L., Grebogi, C.: Erosion of the safe basin for the transversal oscillations of a suspension bridge. Chaos, Solitons Fractals **18(**4), 829–841 (2003)
48. Soliman, M.S., Gonçalves, P.B.: Chaotic behaviour resulting in transient and steady state instabilities of pressure-loaded shallow spherical shells. Journal of Sound and Vibration **259**, 497–512 (2003)
49. Gonçalves, P.B., Silva, F.M.A., Rega, G., Lenci, S.: Global dynamics and integrity of a two-dof model of a parametrically excited cylindrical shell. Nonlinear Dynamics **63**, 61–82 (2011)

50. Silva, F.M.A., Gonçalves, P.B., Del Prado, Z.J.G.N.: An alternative procedure for the non-linear vibration analysis of fluid-filled cylindrical shells. Nonlinear Dyn **66**(3), 303–333 (2011)
51. Silva, F.M.A., Gonçalves, P.B., Del Prado, Z.J.G.N.: Influence of physical and geometrical system parameters uncertainties on the nonlinear oscillations of cylindrical shells. Journal of the Brazilian Society of Mechanical Sciences and Engineering **34**, 622–632 (2012)
52. Rodrigues, L., Silva, F.M.A., Gonçalves, P.B., Del Prado, Z.J.G.N.: Effects of modal coupling on the dynamics of parametrically and directly excited cylindrical shells. Thin Walled Structures **81**, 210–224 (2014)
53. Silva, F.M.A., Brazão, A.F., Gonçalves, P.B., Del Prado, Z.J.G.N.: Influence of physical and geometrical uncertainties in the parametric instability load of an axially excited cylindrical shell. Mathematical Problems in Engineering, Article ID 758959 (2015)
54. Silva, F.M.A., Soares, R.M., Del Prado, Z.J.G.N., Gonçalves, P.B.: Intra-well and cross-well chaos in membranes and shells liable to buckling. Nonlinear Dyn. (2020)().,-volV()0123456789().,-volV)
55. Coaquira, J.C., Cardoso, D.C.T., Gonçalves, P.B., Orlando, D.: Parametric instability and nonlinear oscillations of an FRP channel section column under axial load, Nonlinear Dyn. (2020)
56. Lenci, S., Rega, G.: Control of pull-in dynamics in a nonlinear thermoelastic electrically actuated microbeam. J. Micromech. Microeng. **16**(2), 390–40 (2006)
57. Alsaleem, F.M., Younis, M.I., Ruzziconi, L.: An experimental and theoretical investigation of dynamical pull-in in MEMS resonators actuated electrostatically. J. Microelectromech. Syst. **19**(4), 794–806 (2010)
58. Alsaleem, F., Younis, M.I.: Integrity analysis of electrically actuated resonators with delayed feedback controller. J. Dyn. Syst. Meas. Control **133**(3), 031011 (2011)
59. Ruzziconi, L., Younis, M.I., Lenci, S.: An electrically actuated imperfect microbeam: Dynamical integrity for interpreting and predicting the device response. Meccanica **48**(7), 1761–1775 (2013)
60. Ruzziconi, L., Lenci, S., Younis, M.I.: An imperfect microbeam under an axial load and electric excitation: Nonlinear phenomena and dynamical integrity. International Journal of Bifurcation and Chaos **23**(2), 1350026-1–17 (2013)
61. Ruzziconi, L., Ramini, A., Younis, M., Lenci, S.: Theoretical prediction of experimental jump and pull-in dynamics in a MEMS sensor. Sensors **14**, 17089–17111 (2014)
62. Belardinelli, P., Sajadi, B., Lenci, S., Alijani, F.: Global dynamics and integrity of a micro-plate pressure sensor. Commun Nonlinear Sci Numer Simulat **69**, 432–444 (2019)
63. Rega, G., Settimi, V.: Bifurcation, response scenarios and dynamic integrity in a singlemode model of noncontact atomic force microscopy. Nonlinear Dynamics **73**(1–2), 101–123 (2013)
64. Settimi, V., Rega, G.: Global dynamics and integrity in noncontacting atomic force microscopy with feedback control. Nonlinear Dynamics **86**(4), 2261–2277 (2016)
65. Settimi, V., Rega, G.: Exploiting global dynamics of a noncontact atomic force microcantilever to enhance its dynamical robustness via numerical control. International Journal of Bifurcation and Chaos **26**, 1630018-1–17 (2016)
66. Chandrashekar, A., Belardinelli, P., Staufer, U., Alijani, F.: Robustness of attractors in tapping mode atomic force microscopy. Nonlinear Dyn **97**, 1137–1158 (2019)
67. Lenci, S., Rega, G.: A procedure for reducing the chaotic response region in an impact mechanical system. Nonlinear Dynamics **15**, 391-409 (1998)
68. Rega, G., Lenci, S.: Bifurcations and chaos in single-d.o.f. mechanical systems: exploiting nonlinear dynamics properties for their control. In: Luongo, A. (ed.) Recent Research Developments in Structural Dynamics, pp. 331-369, Research Signpost, Kerala, (2003)
69. Rega, G., Lenci, S.: Identifying, evaluating, and controlling dynamical integrity measures in nonlinear mechanical oscillators. Nonlinear Analysis: Real World Applications **63**, 902-914 (2005)
70. Lenci, S., Rega, G.: Controlling nonlinear dynamics in a two-well impact system. I. Attractors and bifurcation scenario under symmetric excitations. Int. J. Bifurcation Chaos **8**, 2387-2408 (1998)
71. Lenci, S., Rega, G.: Controlling nonlinear dynamics in a two-well impact system. II. Attractors and bifurcation scenario under unsymmetric optimal excitations. Int. J. Bifurcation Chaos **8**, 2409-2424 (1998)
72. Lenci, S., Rega, G.: Optimal numerical control of single-well to cross-well chaos transition in mechanical systems. Chaos Solitons & Fractals **15**, 173-186 (2003)
73. Lenci, S., Rega, G.: Global optimal control and system-dependent solutions in the hardening Helmholtz-Duffing oscillator. Chaos Solitons & Fractals **21**, 1031-1046 (2004)
74. Lenci, G., Rega, S.: Optimal control and anti-control of the nonlinear dynamics of a rigid block. Philosophical Transactions of the Royal Society A: Mathematical, Physical & Engineering Sciences **364**, 2353-2381 (2006)

75. Lenci, S., Rega, G.: Control of the homoclinic bifurcation in buckled beams: infinite-dimensional vs reduced-order modeling. Int. J. Non-Linear Mechanics **43**, 474-489 (2008)
76. Orlando, D., Gonçalves, P.B., Lenci, S., Rega, G.: Increasing practical safety of Von Mises truss via control of dynamic escape. Applied Mechanics and Materials **849**, 46-56 (2016)
77. Rega, G., Lenci, S.: A global dynamics perspective for system safety from macro- to nanomechanics: Analysis, control, and design engineering. Applied Mechanics Reviews **67**, 050802-1–19 (2015)
78. Gonçalves, P.B., Orlando, D., Lenci, S., Rega, G.: Nonlinear dynamics, safety and control of structures liable to interactive unstable buckling. In: S. Lenci, S., Rega, G. (eds.) Global nonlinear dynamics for engineering design and system safety. CISM Courses and Lectures 588, pp. 167-228, Springer Nature (2018)
79. Settimi, V., Rega, G.: Local versus global dynamics and control of an AFM model in a safety perspective. In: Lenci, S., Rega, G. (eds.) Global nonlinear dynamics for engineering design and system safety. CISM Courses and Lectures 588, pp. 229-286, Springer Nature (2018)
80. Dudkowski, P., Jafari, S., Kapitaniak, T., Kuznetsov, N.V., Leonov, G.A., Prasad, A.: Hidden attractors in dynamical systems. Phys. Rep. **637**, 1-50 (2016).
81. Menck, P.J., Heitzig, J., Marwan, N., Kurths, J.: How basin stability complements the linear-stability paradigm. Nat. Phys. **9**(2), 89–92 (2013)
82. Hellmann, F., Schultz, P., Grabow, C., Heitzig, J., Kurths, J.: Survivability of deterministic dynamical systems. Scientific Reports **6** (2016)
83. Daza, A., Wagemakers, A., Georgeot, B., Guery-Odelin, D., Sanjuan, M.A.F.: Basin entropy: A new tool to analyze uncertainty in dynamical systems. Sci. Rep. **6**, 31416 (2016)
84. Brzeski, P., Lazarek, M., Kapitaniak, T., Kurths, J., Perlikowski, P.: Basin stability approach for quantifying responses of multistable systems with parameters mismatch. Meccanica **51**(11), 2713–2726 (2016)
85. Brzeski, P., Wojewoda, J., Kapitaniak, T., Kurths, J., Perlikowski, P.: Sample-based approach can outperform the classical dynamical analysis – experimental confirmation of the basin stability method. Sci. Rep. **7**, 6121 (2017)
86. Brzeski, P., Belardinelli, P., Lenci, S., Perlikowski, P.: Revealing compactness of basins of attraction of multi-DoF dynamical systems. Mechanical Systems and Signal Processing **111**, 348–361 (2018)
87. Brzeski, P. Perlikowski, P.: Sample-based methods of analysis for multistable dynamical systems. Archives of Computational Methods in Engineering **26**, 1515–1545 (2019)
88. Brzeski, P., Kurths, J., Perlikowski, P.: Time dependent stability margin in multistable systems. Chaos **28**, 093104 (2018)
89. Settimi, V., Gottlieb, O., Rega, G.: Asymptotic analysis of a noncontact AFM microcantilever sensor with external feedback control. Nonlinear Dynamics **79**(4), 2675–2698 (2015)
90. Settimi, V., Rega, G.: Influence of a locally-tailored external feedback control on the overall dynamics of a noncontact AFM model. Int. J. Non-Linear Mechanics **80**, 144–159 (2016)
91. Settimi, V., Rega, G., Lenci, S.: Analytical control of homoclinic bifurcation of the hilltop saddle in a noncontact atomic force microcantilever. Procedia IUTAM **19**, 19–26 (2016)
92. Lenci, S., Brocchini, M., Lorenzoni, C.: Experimental rotations of a pendulum on water waves. J. Comput. Nonlinear Dyn. **7**, 011007 (2012)
93. Lenci, S., Rega, G., Ruzziconi, L.: Dynamical integrity as a conceptual and operating tool for interpreting/predicting experimental behavior. Philosophical Transactions of the Royal Society of London A **371**(1993), 20120423-1–19 (2013)
94. Ruzziconi, L., Younis, M.I., Lenci, S.: Dynamical integrity for interpreting experimental data and ensuring safety in electrostatic MEMS. In: Wiercigroch, M., Rega, G. (eds.) IUTAM Symposium on Nonlinear Dynamics for Advanced Technologies and Engineering Design. IUTAM Bookseries 32, pp. 249–261, Springer (2013)
95. Ruzziconi, L., Lenci, S., Younis, M.I.: Interpreting and predicting experimental responses of micro and nano devices via dynamical integrity. In: Lenci, S., Rega, G. (eds.) Global nonlinear dynamics for engineering design and system safety. CISM Courses and Lectures 588, pp. 113–166, Springer Nature (2018)
96. van Campen, D.H., van de Vorst, E.L.B., van der Spek, J.A.W., de Kraker, A.: Dynamics of a multi-dof beam system with discontinuous support. Nonlinear Dyn. **8**(4), 453–466 (1995)
97. Kreuzer, E., Lagemann, B.: Cell mapping for multi-degree-of-freedom-systems parallel computing in nonlinear dynamics. Chaos, Solitons Fractals **7**(10), 1683–1691 (1996)
98. Eason, R., Dick, A.J.: A parallelized multi-degrees-of-freedom cell map method. Nonlinear Dyn. **77**(3), 467–479 (2014)

99. Xiong, F.R., Qin, Z.C., Ding, Q., Hernández, C., Fernandez, J., Schütze, O., Sun, J.Q.: Parallel cell mapping method for global analysis of high-dimensional nonlinear dynamical systems. J. Appl. Mech. **82**(11), 111010 (2015).
100. Xiong, F.R., Han, Q., Hong, L., Sun, J.Q.: Global analysis of nonlinear dynamical systems. In: Lenci, S., Rega, G. (eds.) Global nonlinear dynamics for engineering design and system safety. CISM Courses and Lectures 588, pp. 287–318, Springer Nature (2018)
101. Belardinelli, P , Lenci, S.: A first parallel programming approach in basins of attraction computation. Int J Non Linear Mech **80**, 76–81 (2016)
102. Belardinelli, P., Lenci, S.: An efficient parallel implementation of cell mapping methods for mdof systems, Nonlinear Dyn. **86**(4), 2279–2290 (2016)
103. Marszal, M., Jankowski, K., Perlikowski, P., Kapitaniak, T.: Bifurcations of oscillatory and rotational solutions of double pendulum with parametric vertical excitation. Math. Probl. Eng. **2014**, 892793 (2014)
104. Carvalho, E.C., Goncalves, P.B., Rega, G., Del Prado, Z.J.G.N.: Influence of axial loads on the nonplanar vibrations of cantilever beams. Shock Vib. **20**(6), 1073–1092 (2013)
105. Carvalho, E.C., Goncalves, P.B., Rega, G., Del Prado, Z.J.G.N.: Nonlinear nonplanar vibration of a functionally graded box beam. Meccanica **49**(8), 1795–1819 (2014)
106. Goncalves, P.B., Silva, F.M.A., and Del Prado, Z.J.G.N.: Global stability analysis of parametrically excited cylindrical shells through the evolution of basin boundaries. Nonlinear Dyn. **50**, 121–145 (2007)
107. Schultz, P., Menck, P.J., Heitzig, J., Kurths, J.: Potentials and limits to basin stability estimation. New J. Phys. **19**, 023005 (2017)
108. Agarwal, V., Yorke, J.A., Balachandran, B.: Noise-induced chaotic-attractor escape route. Nonlinear Dyn. **65**, 1–11 (2020)
109. Benedetti, K.C.B., Gonçalves, P.B.: Nonlinear response of an imperfect microcantilever static and dynamically actuated considering uncertainties and noise. Nonlinear Dyn. (2021), submitted
110. Wiercigroch, M., Pavlovskaia, E.: Non-linear dynamics of engineering systems. International Journal of Non-Linear Mechanics **43**(6), 459–461 (2008)
111. Wiercigroch, M., Rega, G.: Introduction to NDATED. In: Wiercigroch, M., Rega, G. (eds.) IUTAM Symposium on Nonlinear Dynamics for Advanced Technologies and Engineering Design. IUTAM Bookseries 32, pp. v–viii, Springer (2013)
112. Szemplinska-Stupnicka, W.: The analytical predictive criteria for chaos and escape in nonlinear oscillators: A survey. Nonlinear Dynamics **7**(2), 129–147 (1995)